UNIVERSITY OF CALIFORNIA, MERCED

MULTI-OBJECTIVE OPTIMAL DESIGN OF CONTROL SYSTEMS

by

Yousef Sardahi

A dissertation submitted in partial satisfaction of the
requirements for the degree of
Doctor of Philosophy

in

Mechanical Engineering

Committee in charge:
Professor Jian-Qiao Sun, Chair
Professor YangQuan Chen
Professor Roummel Marcia

The dissertation of Yousef Sardahi is approved:

Jian-Qiao Sun, Chair Date

YangQuan Chen Date

Roummel Marcia Date

University of California, Merced

To my parents, wife, children and
role-model Professor Jian-Qiao Sun.

ACKNOWLEDGEMENTS

Firstly, I would like to express my sincere gratitude to my advisor Professor Jian-Qiao Sun for the continuous support of my Ph.D. study and related research, for his patience, motivation, and immense knowledge. His guidance helped me in all the time of research and writing of this thesis. I could not have imagined having a better advisor and mentor for my Ph.D. study.

Besides my advisor, I would like to thank the rest of my thesis committee: Professor YangQuan Chen and Professor Roummel Marcia, for their insightful comments and encouragement, but also for the hard question which pushed me to widen my research from various perspectives.

My sincere thanks also goes to Dr. Yousef Naranjani , Mr. Carlos Hernández, Dr. Fu-Rui Xiong, Dr. Yuan Yao, and Mr. Wei Liang, who cooperated, helped and inspired me to finish this work. Without their precious support it would not be possible to conduct this research.

Finally, I would like to thank my parents, wife and children for their unconditional love and support. To my father, I have always wanted you to be proud of me and promised to earn the Ph.D. degree and here I am fulfilling this promise today.

CURRICULUM VITAE

Education

B.S. in Mechatronics Engineering, University of Jordan (Jordan), 2007.

M.S. in Mechanical Engineering (Mechatronics), Jordan University of Science and Technology (Jordan), 2011.

Honors

ME Bobcat Fellowship for the Summer 2016
Travel Award Fellowship 2016
ME Bobcat Fellowship for the Summer 2015
Travel Award Fellowship 2015
ME Bobcat Fellowship for the Summer 2014
Travel Award Fellowship 2014
UCM Summer Fellowship 2013

Publications

Yousef Sardahi, Jian-Qiao Sun (2016) “Many-objective Optimal Design of Sliding Mode Controls”. Accepted in the ASME Journal of Dynamic Systems, Measurement and Control.

Yousef Sardahi, Jian-Qiao Sun (2016) “Many-objective Optimal and Robust Design of PID Controls with a State Observe”. Submitted to Journal of Dynamic Systems, Measurement and Control.

Yousef Sardahi, Yuan Yao, Jian-Qiao Sun (2016) “Multi-objective Optimal Control of Under-actuated Bogie System of High Speed Trains”. Submitted to the International Journal of Vehicle Mechanics and Mobility.

Yousef Sardahi, Yousef Naranjani , Wei Liang, Fu-Rui Xiong, Zhi-Chang Qin, Yang Xue, Carlos Hernández, Oliver Schütze, Jian-Qiao Sun (2013) “Multi-objective Optimal Design of Feedback Controls for Dynamical Systems Time Delay”. *Proceedings of CSTAM CONFERENCE.*

Yousef Sardahi, Yousef Naranjani , Wei Liang, Jian-Qiao Sun, Carlos Hernández and Oliver Schütze (2013) “Multi-objective Optimal Control Design with the Simple Cell Mapping Method". *Proceedings of ASME 2013 International Mechanical Engineering Congress & Exposition. San Diego, California. IMECE2013-65506.*

Yousef Sardahi, Yousef Naranjani , YangQuan Chen, Jian-Qiao Sun "Multi-Objective Optimization of Time-Delayed Fractional-Order Damping for Better Step Response". *Proceedings of the ASME 2015 International Mechanical Engineering Congress and Exposition IMECE2015, November 13-19, 2015, Houston, Texas; 11/2015*

Yousef Naranjani , **Yousef Sardahi**, YangQuan Chen, Jian-Qiao Sun (2015) "Multi-Objective Optimization of Distributed-Order Fractional Damping". *Communications in Nonlinear Science and Numerical Simulation.* 24(1:3), 159-168.

Yousef Naranjani , **Yousef Sardahi**, Jian-Qiao Sun, Hernández and Oliver Schütze (2013) "Fine Structure of Pareto Front of Multi-objective Optimal Feedback Control Design". *Proceedings of the 2013 ASME Dynamic Systems and Control Conference - Control, Monitoring, and Energy Harvesting of Vibratory Systems. Stanford, California. DSCC2013-3944.*

Yousef Naranjani , **Yousef Sardahi**, Jesús Fernández, Oliver Schütze and Jian-Qiao Sun (2014) "A Simple Cell Mapping and Genetic Algorithm Hybrid Method for Multi-Objective Optimization Problems". *EVOLVE-A Bridge between Probability, Set Oriented Numerics, and Evolutionary Computation V.*

Yousef Naranjani , **Yousef Sardahi**, Jian-Qiao Sun (2014) A Genetic Algorithm and Cell Mapping Hybrid Method for Multi-objective Optimization Problems". 11th International Conference on Electrical Engineering, Computing Science and Automatic Control (CCE).

TABLE OF CONTENTS

Chapter

Appendix

LIST OF FIGURES

LIST OF TABLES

ABSTRACT

Feedback controls are usually designed to achieve multiple and often conflicting performance goals. These incommensurable objectives can be found in both time and frequency domains. For instance, one may want to design a control system such that the closed-loop system response to a step input has a minimum percentage overshoot (M_p), peak time (t_p), rise time (t_r), settling time (t_s), tracking error, and control effort (E_u). Another designer may want the controlled system to have a maximum crossover frequency (ω_c), maximum phase margin (P_m) and minimum steady-state error (e_{ss}). However, Most of these objectives cannot be achieved concurrently. Therefore, trade-offs have to be made when the design objective space includes two or more conflicting objectives. These compromise solutions can be found by techniques called multi-objective optimization algorithms. Unlike the single optimization methods which return only a single solution, the multi-objective optimization algorithms return a set of solutions called the Pareto set and a set of the corresponding objective function values called the Pareto front.

In this thesis, we present a multi-objective optimal (MOO) design of linear and nonlinear control systems using two algorithms: the non-dominated sorting genetic algorithm (NSGA-II) and a multi-objective optimization algorithm based on the simple cell mapping. The NSGA-II is one of the most popular methods in solving multi-objective optimization problems (MOPs). The cell mapping methods were originated by Hsu in 1980s for global analysis of nonlinear dynamical systems that can have multiple steady-state responses including equilibrium states, periodic motions, and chaotic attractors. However, this method can be also used also to solve multi-objective optimization problems by using a direct search method that can steer the search into any pre-selected direction in the objective space.

Four case studies of robust multi-objective/many-objective optimal control design are introduced. In the first case, the NSGA-II is used to design the gains of a PID (proportional-integral-derivative) control and an observer simultaneously. The optimal design takes into account the stability robustness of both the control system and the estimator at the same time. Furthermore, the closed-loop system's robustness against external disturbances and measurement noises are included in the objective space.

The second case study investigates the MOO design of an active control system applied to an under-actuated bogie system of high speed trains using the NSGA-II. Three conflicting objectives are considered in the design: the controlled

system relative stability, disturbance rejection and control energy consumption. The performance of the Pareto optimal controls is tested against the train speed and wheel-rail contact conicity, which have huge impact on the bogie lateral stability.

The third case addresses the MOO design of an adaptive sliding mode control for nonlinear dynamic systems. Minimizing the rise time, control energy consumption, and tracking integral absolute error and maximizing the disturbance rejection efficiency are the objectives of the design. The solution of the MOP results in a large number of trade-off solutions. Therefore, we also introduce a post-processing algorithm that can help the decision-maker to choose from the many available options in the Pareto set.

Since the PID controls are the most used control algorithm in industry and usually experience time delay, a MOO design of a time-delayed PID control applied to a nonlinear system is presented as the fourth case study. The SCM is used in the solution of this problem. The peak time, overshoot and the tracking error are considered as design objectives and the design parameters are the PID controller gains.

Chapter 1

INTRODUCTION

The process of optimizing two objectives or more simultaneously is called multi-objective optimization or vector optimization. In some references when the number of objectives are more than three, the term many-objective optimization is used instead.

Most real-life problems have several conflicting criteria that have to be considered at the same time. For example, one may want to buy the cheapest and the most comfortable car. However, these two goals cannot be achieved at the same time. So, the problem of minimizing the cost and maximizing the comfort when buying a car can be formulated as a multi-objective optimization problem with two conflicting objectives. Another example of conflicting criteria that can be found in real-life applications is maximizing performance whilst minimizing fuel consumption and emission of pollutants when designing a vehicle. These three incommensurable aims cannot be satisfied concurrently and trade-offs need to be made among them.

One can notice that since the objectives are in competition, the traditional single objective optimization and linear programming algorithms are not enough. Because the solution of these kinds of problems is not a single point, but rather a set of solutions, which represents the trade-offs between cost and comfort in the case of buying a car or performance, fuel consumption and emission of pollutants while designing a vehicle. Therefore, in real-life applications one is faced with the problem of finding the best trade-off solutions for the given problems.

1.1 Multi-Objective Optimization

Multi-objective Optimization Problems (MOPs) have been in focus for a long time because of their vast applications. The solutions to MOPs are not certain points, but rather it forms a set called *Pareto set* and the set of corresponding objective function values is called *Pareto front*. A MOP problem can be expressed as follows:

$$\min_{\mathbf{k}\in Q}\{\mathbf{F}(\mathbf{k})\}, \tag{1.1}$$

where $\mathbf{F}$ is the map that consists of the objective functions $f_i : Q \to \mathbf{R}^1$ under consideration.

$$\mathbf{F} : Q \to \mathbf{R}^k,\ \mathbf{F}(\mathbf{k}) = [f_1(\mathbf{k}), \dots, f_k(\mathbf{k})]. \tag{1.2}$$

$\mathbf{k} \in Q$ is a q-dimensional vector of design parameters. The domain $Q \subset \mathbf{R}^q$ can in general be expressed by inequality and equality constraints:

$$\begin{aligned} Q \ &= \{\mathbf{k} \in \mathbf{R}^q \mid g_i(\mathbf{k}) \leq 0,\ i = 1, \ldots, l, \\ &\qquad \text{and } h_j(\mathbf{k}) = 0,\ j = 1, \ldots, m\}. \end{aligned} \tag{1.3}$$

The concept of *dominancy* [1] which is defined below, plays an important role in defining the optimal solution of a given MOP:

1.1.1 Definition 1

(a) Let $\mathbf{v}, \mathbf{w} \in \mathbf{R}^k$. The vector $\mathbf{v}$ is said to be *less than* $\mathbf{w}$ (in short: $\mathbf{v} <_p \mathbf{w}$), if $v_i < w_i$ for all $i \in \{1, \ldots, k\}$. The relation $\leq_p$ is defined analogously.

(b) A vector $\mathbf{v} \in Q$ is called *dominated* by a vector $\mathbf{w} \in Q$ ($\mathbf{w} \prec \mathbf{v}$) with respect to the MOP (1.1) if $\mathbf{F}(\mathbf{w}) \leq_p \mathbf{F}(\mathbf{v})$ and $\mathbf{F}(\mathbf{w}) \neq \mathbf{F}(\mathbf{v})$, else $\mathbf{v}$ is called non-dominated by $\mathbf{w}$.

If a vector $\mathbf{w}$ dominates a vector $\mathbf{v}$, then $\mathbf{w}$ can be considered to be a ‘better’ solution of the MOP. The definition of optimality or the ‘best’ solution of the MOP is now straightforward.

1.1.2 Definition 2

(a) A point $\mathbf{w} \in Q$ is called *Pareto optimal* or a *Pareto point* of the MOP (1.1) if there is no $\mathbf{v} \in Q$ which dominates $\mathbf{w}$.

(b) The set of all Pareto optimal solutions is called the *Pareto set* denoted as

$$\mathcal{P} := \{\mathbf{w} \in Q : \mathbf{w} \text{ is a Pareto point of the MOP (1.1)}\}. \tag{1.4}$$

(c) The image $\mathbf{F}(\mathcal{P})$ of $\mathcal{P}$ is called the *Pareto front.*

Pareto set and *Pareto front* typically form $(k-1)$-dimensional manifolds under certain mild assumptions on the MOP. A survey of the methods for the solution of MOPs can be found in [2,3]. In the next section, only the MOP methods that have been used in the design of control systems will be discussed.

1.2 MOP Methods Used in Control Systems Design

There are many methods for solving MOPs. These methods can be classified into two or more categories. See, for example, the references [4–7]. In [4], the methods were divided into two groups: generation methods and preference-based methods. In the former category, the solution set is generated first. Then, the optimal solution is introduced to the decision maker who has the absolute authority to choose any point from it, reject the whole solution or accept it. In the latter category, the decision maker must specify preferences regarding the objective functions articulated in terms of goals, importance of objectives, *etc.* These preferences are taken into account during the solution process and the solution that best satisfies the user's preferences is elected.

Another classification can be found in [7] where the MOP techniques are put into four categories: no-preference, posterior, prior and interactive methods.

In this thesis, we adopt the classification presented in [8] where the MOP approaches are split into three categories: scalarization, Pareto, and non-scalarization non-Pareto methods. It is worth mentioning that the first two categories are the most important MOP techniques [8, 9].

1.2.1 Scalarization Methods

The scalarization methods require transformation of the MOP into a single optimization problem (SOP), normally by using coefficients, exponents, constraint limits, *etc.* and then methods for single objective optimization are utilized to search for a single solution. Computationally, these methods find a unique solution efficiently and converge quickly. However, these methods cannot discover the global Pareto solution for non-convex problems [9]. Also, it is not always obvious for the designer to know how to choose the weighting factors for the scalarization [7, 9].

There are three common scalarization methods reported in the literature. They are the weighted sum approach [10, 11], goal attainment method [12] and lexicographic method [13].

The weighted sum approach is perhaps one of the commonly used methods [9]. It is based on adding the weighted objectives to form a single cost function as follows,

$$\min_{\mathbf{k}\in Q} \sum_{i=1}^{n} w_i f_i(\mathbf{k}), \tag{1.5}$$

where, $w_i > 0$ for all $i = 1, ..., n$ and $\sum_{i=1}^{n} w_i = 1$. The optimization may be also subjected to various constraints. The objective functions are often normalized in the weighted sum when they have different range of values.

A clear advantage of this method is that the SOP methods can be used to produce a unique solution, which also means that the solution can be found by less computational burden. However, the weighting factors have a huge impact on the solution and they are hard to be selected [9]. It is also worth mentioning that these "weights indicate the relative importance of the corresponding objective function but they do not mean priorities" [9]. Other drawback of this method is that the optimization process becomes very difficult in case of non-convex problems [7, 9].

The goal attainment method includes a set of prior chosen design targets. Each target is associated with an objective. The formulation of the MOP in this case allows the objectives to be under- or over-achieved so that the initial design goals can be chosen to be imprecise by the decision-maker. The relative degree of under- or over-achievement of these targets is determined by a set of weighting factors. A standard optimization problem using this method can be given as follows,

$$\min_{\gamma \in \mathbf{R}^1,\ \mathbf{k} \in Q} \gamma, \tag{1.6}$$

such that $f_i(\mathbf{k}) - w_i\gamma \leq f_i^*(\mathbf{k})$ subject to other constraints. Here, $f_i(\mathbf{k})$ are objective functions, w_i are weights indicating the relative importance of each objective function. This vector has to be elected by the decision maker before the MOP method is applied. $f_i^*(\mathbf{k})$ are the goals, which have to be reached, and γ is an unrestricted scalar.

It is evident that this method shares similar properties with the weighted sum method, where the most important task is to find the weight vector. Also, each element in this vector does not represent the corresponding function priority.

In the lexicographic method, objective functions are sorted according to their importance, starting with the most important one to the least. A MOP of this method can be formulated as follows [7],

$$\min_{\mathbf{k} \in Q} f_1(\mathbf{k}), f_2(\mathbf{k}), ..., f_n(\mathbf{k}), \tag{1.7}$$

where f_1 is the most important and f_n is the least important objective.

The merit of this approach is that there is only one unique solution for a given lexicographic order. Also, the implementation of this method is straightforward because of the sequential optimization. Its demerit is that usually criteria with lower priorities will not be satisfied. Therefore, priority assignment is of great importance for the success of this technique [9].

1.2.2 Pareto Methods

Unlike the scalarization methods, the Pareto methods do not aggregate the elements of the objectives into a single fitness function. They keep the objectives separate all the time during the optimization process. Therefore, they can handle all conflicting design criteria independently, and compromise them simultaneously [9]. The dominancy concept in Section 1.1 is used to differentiate between inferior and non-inferior solutions. The Pareto methods provide the decision-maker with a set of solutions such that every solution in the set expresses a different trade-off among the functions in the objective space. Then, the decision-maker can select any point from this set. In other words, in contrast to the scalarization methods where the preferences have to be expressed before the optimization is carried out, in the Pareto methods, these preferences can be decided once the optimization process is over [7, 9, 14].

Compared to the scalarization approaches, the Pareto methods can successfully find the optimal or near-optimal solution set. They are computationally more expensive. In general, these methods can be classified into three classes: multi-objective evolutionary algorithm (MOEAs), multi-objective deterministic methods and multi-objective hybrid methods.

Evolutionary algorithms are most broadly used for MOPs [15]. The basic notion in evolutionary computation is to evolve an entire set of trial solutions of chosen size toward the solution during the search. Evolutionary algorithms designed for these problems have been demonstrated their power in many applications. The solution set can be well approximated in most cases with these algorithms [16].

The first attempt of using MOEAs in solving MOPs was circa 1988 in [17]. Since then, many MOEAs were developed. The most important are: ACO (Ant Colony Optimization, [18]), MOGA (Multiple Objective Genetic Algorithm, [19]), PSO (Particle Swarm Optimization, [20]), NSGA-II (Non-dominated Sorting Genetic Algorithm, [21]), SPEA2 (Strength Pareto Evolutionary Algorithm, [22]), and NPGA-II (Niched Pareto Genetic Algorithm, [23]). Mainstream evolutionary algorithms for MOPs include genetic algorithm (GA), multi-objective particle swarm optimization (MOPSO) and strength Pareto evolutionary algorithm (SPEA).

Deterministic methods such as set oriented methods with subdivision techniques [24], and MOO algorithm based on the simple cell mapping (SCM) [16] can be used to find the solution set. The advantage of the set oriented methods is that they produce an approximation of the global Pareto set in one single run of the algorithm. The cell mapping method is the predecessor of the set oriented methods, and was proposed in [25] for global analysis of nonlinear dynamic systems. It can be also implemented with subdivision techniques. Both of these approaches can be used to solve optimization problems and are characterized by a great robustness. Therefore, these techniques are attractive choices against ‘classical’ mathematical programming approaches, specially for solving low or moderate dimensional problems.

Even though the study of hybrids of MOO techniques is still relatively scarce, this topic is receiving much attention. The aim of the hybridization is to reduce the number of function evaluations and improve the quality and diversity of the solution. For instance, a hybrid approach of a fast differential evolution multi-objective algorithm and a local search method based on the use of rough set theory is introduced [26]. The new algorithm has less computational cost and is robust in solving difficult constrained multi-objective optimization problems as compared to NSGA-II.

Other examples have been also reported in the literature. In [27], a genetic algorithm is coupled with a tabu search. A hybridization of simulated annealing principles with genetic algorithms is studied in [28] and [29]. More details about hybrid MOP methods can be found in [30].

1.2.3 Non-Pareto and Non-scalarization Methods

There are two MOO algorithms that cannot be classified as either Pareto or scalarization Methods. They are the $\epsilon-$constraint method [31] and the VEGA (Vector Evaluated Genetic Algorithm, [32]) approach.

The $\epsilon-$constraint method was proposed in 1971 by Haimes. In this method, one of the cost functions is selected to be optimized and the rest of the functions in the objective space are converted into constraints by setting an upper bound to each of them. In this case, the MOP is formulated as follows

$$\begin{gathered} \min f_l(\mathbf{k}), \\ \text{subject to } f_j(\mathbf{k}) \leq \varepsilon_j \ldots \text{for all } j = 1, ..., n, \quad n \neq l \end{gathered} \tag{1.8}$$

The VEGA works almost in the same way as the single objective genetic algorithm. Its selection step has been modified. In this step, a number of subpopulations is produced at each generation. These subpopulations are resulted from performing proportional selection according to each objective function. For Instance, for a problem with k objectives and N population size, k subpopulations of size N/k each are created. These subpopulations are then combined to form a new population of size N. After that, the crossover and mutation processes are applied as in the standard GA.

One of the disadvantages of this algorithm is that it does not perform well in the case of a concave trade-off surface where the population tends to split into different species. Each of them is particularly strong in one of the objectives. This phenomenon is not desirable because it disagrees with the goal of finding a compromised solution [33].

These algorithms have been exploited in the design of multi-objective optimal linear and nonlinear controls. In the next section, we list some of these examples.

1.3 The State-of-the-art of MOPs in Control Systems

Multi-objective optimal control has been receiving much attention. Examples can be found in almost all the control fields including linear, robust, nonlinear and structural control systems [34].

In linear control systems, the multi-objective optimal design of the proportional-integral-derivative (PID) controller has the lion share of the literature. Because of vast applications of PID controls in industries, there have been many studies to develop designs or tuning techniques of the control. The multi-objective optimal design of this type of control systems is discussed extensively in [14]. For the last three decades, there have been a large number of publications on multi-objective optimal design of PID controllers. For instance, in [35], a MOGA is used to design a fixed-gain PID controller and a gain-scheduled PID for a highly nonlinear chemical pilot plant. Two design objectives are considered: minimum integral square error (ISE)

and minimum control effort defined by $|u|$, where u is the control signal. In [36] , an algorithm called the global ranking genetic algorithm was developed and used to design the PID controller gains for a rotary inverted pendulum. Three conflicting functions are considered in the design including the settling time, overshoot and mean square steady-state error. Another multi-objective genetic algorithm called the genetic artificial immune system algorithm was investigated in [37]. The four fitness functions are considered: the rise time, overshoot, settling time, and integral square error. A non-dominated sorting genetic algorithm was used in [38] to tune the control gains to minimize the rise time, overshoot and settling time. Similar multi-objective optimal control designs are studied with different algorithms for multi-objective optimization problems including the ant colony algorithm [39], an immune algorithm [40] and the imperialist competitive algorithm [41]. One of the most important works in the field of MOPs of PID controller is proposed in [42], where four objectives, overshoot, rise time, settling time and J_{IAE} (Integral absolute error), are optimized using NSGA-II. A similar design method is introduced in [43], but the solution is found by using a gradient-based MOP algorithm.

Other designs are done in the frequency domain where the gain and phase margins are used to characterize the system stability and robustness, and the crossover frequency is used to assess the system speed of response [44]. For example, an optimal PID control designed in the frequency domain and applied to a rotary hydraulic system has been proposed in [45]. The control parameters are tuned such that the crossover frequency, gain margin, phase margin, and steady state error are within targeted ranges. In [46], a PI controller is design by optimizing three objective functions: weighted integral square error, gain and phase margins. The goal attainment method is used to solve this problem for two different case studies: the first order plus delay time (FOPDT) models and integrator plus delay time (IPDT) models.

The first attempt to use nonlinear optimization methods in robust control was reported in [47]. Therein, the weights for LQG (Linear-Quadratic-Gaussian) control design was tuned using a method called DELIGHT which is an interactive optimization-based method. A similar idea was proposed in [48].Therein, LQG (Loop Transfer Recover) LTR weighting matrices are designed by using Matlab's constrained optimization function. These matrices are computed such that a user defined performance criterion is minimized under both performance and stability robustness constraints. Another example is found in [49] where the problem of designing a robust control system for a distillation column is formulated as a constrained MOP problem. The MOP performance indices include the individual eigenvalue sensitivities, and the sensitivity and the complementary sensitivity functions in the frequency domain. The robust performance criteria are formulated as a set of inequalities and the full-state feedback matrix are designed by using genetic algorithm. A robust H_∞ control for rotorcraft is designed using multi-objective particle swarm optimization has been reported in [50]. The algorithm minimizes three functionsrising time, overshoot, and bandwidth while it searches for the optimal parameters of three frequency-dependent weighting functions- the performance weighting function, control activity weighting function and robustness weighting function-under the circumstance of the given structures of three weighting matrices in the H_∞ mixed sensitivity design.

Although up to now only limited studies on multi-objective design of nonlinear control systems have been done, several prosperous applications of common stochastic algorithms such particle swarm optimization (PSO) [51] and the genetic algorithm [52] show an increasing interest in this subject. A multi-objective optimization on sliding surface construction by using genetic multi-objective algorithm was investigated in [53]. In [54], a hybrid fuzzy and genetic algorithm-based multi-objective optimization approach was used to tune the parameters of sliding mode control (SMC) applied to a remotely operated underwater vehicle system. SMC to train neural networks for multi-objective optimization was developed in [55]. In [56], non-dominated multi-objective genetic algorithm (NSGA-II) is used to optimize parameters of membership functions and find appropriate fuzzy rules of a fuzzy logic controller implemented on a smart base-isolation system which consist of a friction pendulum system and a large magnetorheological damper. In [57], three control techniques: skyhook control, feedback linearization, and sliding mode control applied to semi-active vehicle suspensions were optimized by the multi-objective genetic algorithm (MOGA). Two objectives were considered: ride quality, as measured by absorbed power, and thermal performance, as measured by power dissipated in the suspension damper. The design parameter space includes only one parameter called skyhook control, feedback, or sliding mode control gain. A comparison study of the Pareto optimal design of the decoupled sliding mode controller for an inverted pendulum system was presented in [58]. In that respect, five different algorithms: the Sigma method [59], the modified NSGA-II algorithm [60], the MOGA toolbox in Matlab and a novel PSO algorithm were used. In [61], an optimal robust sliding mode tracking control of a biped robot was designed by a new variant of PSO algorithm called ingenious multi-objective PSO. To show the superiority of the new algorithm, the same control problem was optimized with three well-known multi-objective optimization algorithms, modified NSGAII, Sigma method, and MOGA. The most recent work in this matter was published in [62]. Therein, a multi-objective optimal sliding mode applied to an under-actuated nonlinear system was designed by the parallel simple cell mapping method. The results demonstrated that the presented multi-objective designs are quite useful.

In [63], a constrained optimization problem with two objectives of actively controlled structures was solved by a hybrid method combined a Pareto genetic algorithm (GA) and a fuzzy penalty function. The Pareto GA with five basic operators: reproduction, crossover, mutation, niche, and the Pareto-set filter was used to find the solution set while the fuzzy penalty function was used to transform the constrained optimization problem into non-constrained one. In [64], the problem of building an actively controlled structure with constraints was formulated as MOP. This method was applied to two truss structures. The objective space had four objective functions: the weight of the structure, control effort in terms of the Frobenious norm of the control gains, effective damping response time, and performance index, which provides a measure of the total system energy. The design space was chosen as the cross-sectional areas of the members of the structure. In [65] , physical programming algorithm was used to design a robust control system for a well-known benchmark control problem, two degree-of-freedom spring-and-mass system. The objective space included five design metrics: settling time, stability, noise amplification, control effort, and controller complexity, which represents the controller order. The size of the design parameter space is nine variables used in the development of the controller.

1.4 Outline of the Thesis

This dissertation is based on the author's research publications on multi-objective optimal design of control systems in the past four years. Two algorithms have been used in the research: the non-dominated sorting genetic algorithm II and a multi-objective optimization algorithm based on the simple cell mapping, which are detailed in Chapter 2 . Chapters 3, 4 and 5 propose multi-objective optimal designs of a PID controller with a state observer, partial state-feedback controller applied to a high speed train, and an adaptive sliding mode controller, respectively. Chapter 6 focuses on the application of MOP algorithm based on the SCM method to the design of a time-delayed PID controller applied to a nonlinear Duffing system. Chapter 7 summarizes the work and suggests the future works.

Chapter 2

MOP ALGORITHMS BASED ON SCM AND NSGA-II

2.1 Introduction

In this chapter, we describe two Pareto algorithms for MOPs. The first one is called the non-dominated sorting genetic algorithm II (NSGA-II) which belongs to the family of stochastic algorithms. This algorithm has been widely used in the literature to solve MOPs. The second one belongs to the family of deterministic methods and is termed the simple cell mapping (SCM) method for MOPs.

2.2 NSGA-II

NSGA developed in [66] is a non-domination based genetic algorithm. Even though it performs well in solving MOPs, its high computational effort, lack of elitism, and the implementation of what is called sharing parameter necessitate improvements. As a result, a modified version of the algorithm named NSGA-II was presented in [67]. The new version has a better sorting algorithm, includes elitism, eliminates the need for the sharing parameter, and has less computational burden.

As shown in Table 2.1, the algorithm incorporates eight basic operations: Initialization, fitness evaluation, non-domination ranking, crowding distance calculation, tournament selection, crossover, mutation, and combination [67].

It starts with the initialization process in which a random population, $Npop$, that satisfies the constraints, $[\mathbf{lb}\ ,\ \mathbf{ub}]$, is generated. Once the population is initialized, fitness function evaluations, $\mathbf{F}(Pop)$, takes place in the second stage.

Using these function values, the candidate solutions are sorted based on their non-domination and placed into different fronts. The realization of this algorithm is shown in Table 2.2. The solutions in the first front dominate all the other individuals while those in the second front are dominated only by the members in the first front. Similarly, the solutions in the third front are dominated by individuals in both the first and second fronts, and so on. Each candidate solution is given a rank number, r, of the front where it resides. For instance, members in first front are ranked 1 and those in second are given a rank of 2 and so on.

To improve the diversity of the solution, a parameter called the crowding distance is computed for each solution as shown in Table 2.3. This parameter measures how close an individual is to its neighbors. In this algorithm, nf denotes the number of individuals in the front and $nobj$ is the number of objective functions. The crowding distance is calculated front wise and comparing the crowding distance between two individuals from two different fronts is meaningless. The larger the average crowding distance, the better the diversity of the population.

After that, the parents for the next generation are selected. The binary tournament selection method, shown in Table 2.4, is used for this purpose. In this algorithm, $randint$ generates two uniform random integers between 1 and $Npop$. These values are used to fetch two candidate parents from **Pop**. A candidate solution is selected if its rank is smaller than the other or if its diversity measure is bigger than the other.

Then, the arithmetic crossover (see Table 2.5) [68, 69] and simple mutation (see Table 2.6) [70] operators are applied on the selected parents to produce new children. These two operations are repeated nc times, where $nc = round(Npop/2)$, and result in a new offspring of size $Npop$. In the mutation algorithm, p_m is the mutation probability which is used to mutate the j^{th} variable of a child with $navrs$ of design parameters when $rand$ (generates a uniform random number between [0 1]) is less than or equal to p_m. Mutation should allow the algorithm to avoid local minima by preventing the population of chromosomes from becoming too similar to each other. Elaborated details about crossover and mutation methods can be found in [71].

After that, the new children is merged with the current population. This combination guarantees the elitism of the best individuals.

Finally, the population is sorted based on the crowding distance, $\mathbf{d}$, and rank, $\mathbf{rnk}_p$, values. First, the sorting is performed with respect to $\mathbf{d}$ in a descending order. Then, an ascending order of the population is followed based on the rank values. The new generation is produced from the sorted population until the size reaches $Npop$.

As long as the number of generations, gen, is not equal to the maximum number of iterations, $Ngens$, the selection, crossover, mutation, merging, ranking and sorting process are repeated.

The NSGA-II converges to the neighborhood of the solution very quickly and slows down subsequently. That is, it needs more time to converge to the global solution of MOPs. It is an attractive choice to high dimensional problems that the number of populations is usually kept to be manageable.

Another algorithm that can approximate the real Pareto solution accurately is the MOP algorithm based on the SCM. This method is a very interesting alternative against ‘classical’ mathematical programming techniques in particular for the thorough investigation of low or moderate dimensional MOPs.

Table 2.1: Algorithm 1 – Pseudo code of NSGA-II

```
INPUT: $\mathbf{F}; nvars; nobj; \mathbf{ub}; \mathbf{lb}; Npop; Ngens; p_m$
OUTPUT: Ps, Pf
1: [Initialization] Generate a random population, Pop, of $Npop$
  chromosomes within the specified constraints, ub and lb.
2: [Fitness] Evaluate multiple fitness of each chromosome
    in the population, $\mathbf{F}(Pop)$
3: [Rank] Rank the population by the following steps:
    3.1 [Domination rank] Rank individuals in population
          by using Algorithm 2.
    3.2 [Crowding distance] Calculate the crowding distance
          by using Algorithm 3.
4: while $gen < Ngens$
5: while $k \leq n_c$
6: $parent_1 \longleftarrow$ Selection($r, d$, Pop)
7: $parent_2 \longleftarrow$ Selection($r, d$, Pop)
8: C_childern $\longleftarrow$ Crossover($nvars, parent_1,\ parent_2$, ub, lb)
9: M_Childern$_1$ $\longleftarrow$ Mutation($navrs$, Crossover_childern$_1$, $p_m$, ub, lb)
10: M_Childern$_2$ $\longleftarrow$ Mutation($navrs$, Crossover_childern$_2$, $p_m$, ub, lb)
11: end while
12:  [Fitness] Evaluate multiple fitness of M_Childern
13:  [Merge] Pop $\longleftarrow$ [Pop, M_Childern]
14: [Rank] by using Algorithm 2 and Algorithm 3.
15: [Sort Population] sort Pop based on their $d$ and $r$
16: [Replace] Pop $\longleftarrow$ Pop($1 : Npop$)
17: end while
18: Ps $\longleftarrow$ Pop
19: Pf $\longleftarrow$ F(Pop)
```

Table 2.2: Algorithm 2 – Pseudo code of domination rank .

```
**INPUT:** $\mathbf{F}; \mathbf{Pop}$
**OUTPUT:** $\mathbf{rnk}$
1: Let rank counter $r$ be zero.
2:  Increase: $r = r + 1$.
3: Find the non-dominated individuals, $\mathbf{S}$, from population $\mathbf{Pop}$
   based on the definition of domination.
4: $\mathbf{rnk}_p \longleftarrow r \; \forall p \in \mathbf{S}$
5: Remove these individuals from $\mathbf{Pop}$ and continue.
6: If $\mathbf{Pop}$ is empty then stop, else go to step 2.
```

Table 2.3: Algorithm 3 – Pseudo code of Crowding distance.

```
**INPUT:** $\mathbf{F}; nf; nobj$
**OUTPUT:** $\mathbf{d}$
1: Let $d_k = 0$ for $k = 1, 2, , nf$.
2:  For each objective function $f_i, i = 1, 2, ...,nobj$
   sort the set in ascending order.
3: Let $d_1$ and $d_{nf}$ be maximum values, e.g. $d_1 = d_{nf} = \infty$.
4: For $j = 2$ to $(nf - 1)$, set $d_j = d_j + \sum_{k=1}^{nobj} \frac{f_i(j+1) - f_i(j-1)}{f_i(nf) - f_i(1)}$.
```

Table 2.4: Algorithm 4 – Pseudo code of the selection method.

```
INPUT: rnk; d; Pop
OUTPUT: parent
$rn \longleftarrow randint(1, 2, [1\ Npop])$
$\mathbf{w} \longleftarrow \mathbf{Pop}(rn_1)$
$\mathbf{u} \longleftarrow \mathbf{Pop}(rn_2)$
if $\mathbf{rnk}(\mathbf{w}) < \mathbf{rnk}(\mathbf{u})$ then
  parent $\longleftarrow$ w
elseif $\mathbf{rnk}(\mathbf{w}) > \mathbf{rnk}(\mathbf{u})$ then
  parent $\longleftarrow$ u
else
  if $\mathbf{d}(\mathbf{w}) < \mathbf{d}(\mathbf{u})$ then
    parent $\longleftarrow$ u
  else
    parent $\longleftarrow$ w
  end if
end if
```

Table 2.5: Algorithm 5 – Pseudo code of crossover.

```
INPUT: $nvars$, $\mathbf{parent}_1$, $\mathbf{parent}_2$; ub; lb
OUTPUT: C_childern
1: Generate uniform random vector, $\alpha$, between [0 1]
$\alpha = \text{rand}_{1\times nvars}$
2: Assign the children's values by the following equations:
$\mathbf{C\_childern}_1 = \alpha \times \mathbf{parent}_1 + (\mathbf{1} - \alpha) \times \mathbf{parent2}$
$\mathbf{C\_childern}_2 = \alpha \times \mathbf{parent}_2 + (\mathbf{1} - \alpha) \times \mathbf{parent1}$
3: Judge whether the obtained value located within the
   available range [lb, ub], if the value beyond, reset
   the chromosome within the available range
```

Table 2.6: Algorithm 6 – Pseudo code of the mutation operator .

```
INPUT: $nvars$;child; $p_m$; ub; lb
OUTPUT: M_Childern
M_Childern = child
while $j \leq nvars$ do
    if $rand \leq p_m$
        M_Childern$_j$ = rand $\in [lb_j; ub_j]$
    end if
```

2.3 Simple Cell Mapping Method

The cell mapping methods describe system dynamics with cell-to-cell mappings by discretizing both the phase space and time. In MOPs, the SCM method is applied to the dynamic search process in the design parameter space, not to the original dynamical system in time domain. The point-to-point mapping obtained from the gradient search algorithm for MOPs can be written as

$$\mathbf{k}(i) = \mathbf{G}(\mathbf{k}(i-1)), \tag{2.1}$$

where $\mathbf{k}(i) \in \mathbf{R}^q$ is the design vector at the i^{th} mapping step. In the SCM, the dynamics of an entire cell denoted as Z is represented by the dynamics of its center. The center of Z is mapped according to the point-to-point mapping. The cell that contains the image point is called the image cell of Z. The cell-to-cell mapping corresponding to Equation (2.1) is denoted by C,

$$Z(i) = C(Z(i-1)). \tag{2.2}$$

To illustrate how the SCM is constructed for MOPs, we present a Directed Search (DS) algorithm [72, 73], which has the benefit of needing less information to perform the local search for minimum, assuming that the parameter space Q is discretized into a collection of finite size cells and that the SCM method is applied.

The first step of the SCM method for MOP is to compute the objective functions at the center point of all the cells in Q. The DS algorithm allows to steer the search into any pre-selected direction $\mathbf{di} \in \mathbf{R}^k$ in the objective space. $\mathbf{di}$ is usually chosen from the current location in the objective function space to point to a direction along which all the objective functions decrease [74]. To apply the gradient free version of this algorithm within SCM, we can proceed as follows: Choose $nb \geq q$ neighboring cells of a current cell under processing. Define unit vectors as

$$\nu_i = \frac{\mathbf{k}_i - \mathbf{k}_0}{\|\mathbf{k}_i - \mathbf{k}_0\|_2} \quad i = 1, 2, \cdots, nb, \tag{2.3}$$

where $\mathbf{k}_0$ is the center of the current cell, and $\mathbf{k}_i$ is the center of the i^{th} cell in the immediate neighborhood of $\mathbf{k}_0$. Define a matrix $\mathcal{F} = \{m_{i,j}\} \in \mathbf{R}^{k \times nb}$ as

$$m_{i,j} = \frac{f_i(\mathbf{k}_j) - f_i(\mathbf{k}_0)}{\|\mathbf{k}_j - \mathbf{k}_0\|_2}, \tag{2.4}$$

which is an approximation of the directional derivative of $f_i(\mathbf{k}_0)$ in direction ν_j at $\mathbf{k}_0$. Compute

$$\lambda = \mathcal{F}^+ \mathbf{di}, \tag{2.5}$$

where $\mathcal{F}^+$ denotes the pseudo inverse of $\mathcal{F}$ [75]. Then a line search in the parameter space along the direction

$$\nu = \sum_{i=1}^{nb} \lambda_i \nu_i, \tag{2.6}$$

leads to a movement along $\mathbf{di}$-direction in the objective space. If the search along ν-direction near the neighborhood of the current cell $\mathbf{k}_0$ ends at a cell $\mathbf{k}_d$ which dominates $\mathbf{k}_0$, i.e. $\mathbf{F}(\mathbf{k}_{di}) \leq_p \mathbf{F}(\mathbf{k}_0)$, $\mathbf{k}_{di}$ is taken as the image cell of $\mathbf{k}_0$. If no such a cell can be found, the current cell $\mathbf{k}_0$ may be on the Pareto set, and we assign its image as itself. This is how the simple cell mappings are constructed for all the cells in the parameter space Q. After all the cells are processed, we apply the sorting algorithm due to Hsu to identify periodic and transient cells in the discretized domain Q [25]. The periodic cells represent an approximation of the Pareto set, with possibly one exception.

If no transient cells are mapped to a periodic cell with period one, the periodic cell is isolated. We change it to be the sink cell. This can happen when a cell is not on the Pareto set and none of its neighboring cells dominates it.

Next, we discuss a hybrid algorithm for computing the SCM of a MOP. The hybrid algorithm consists of a gradient free search on a relatively coarse cell space and a gradient based search on the region of the approximate Pareto set obtained by the gradient free search with much refined cells. For the gradient free search, the image of a cell is selected by comparing the objective function values of all its neighboring cells. If there is only one dominant cell in the neighborhood, it becomes the image of the cell under consideration. If there are more than one dominant cells, we select the one that has the highest objective function value decrease per unit distance. Such a choice mimics the steepest gradient decent algorithm. The outcome of the gradient free search on a coarse cell partition is a covering set of the Pareto set.

We point out that gradient based approaches could be realized efficiently in the context of SCM. If the cells are small enough, one could, for instance, use the center points of the neighboring cells to obtain a finite difference approximation of the gradient at a given cell. This would in principle open the door for the usage of all gradient based search algorithms, but without explicitly computing the gradient. Since the function values for the center points of neighboring cells in all q directions are already known, the approximation of the gradient comes for free in terms of the additional function evaluations. This is the reason that a gradient search algorithm is proposed for the second step of the hybrid algorithm over the refined cell space.

Before the refinement step in the hybrid algorithm, we programmatically make the covering set larger than the collection of all periodic cells by including their immediate neighboring cells. This is a strategy to avoid the missing segments of the Pareto set. As a final step, the dominance of the cells in the Pareto set is checked in order to remove the additional cells that are brought in to avoid the missing segments of the Pareto set.

We should note that the exact image of the center of a cell is approximated by the center of its image cell. This approximation can cause significant errors in the long term solution of dynamical systems [76–78]. The cell mapping with a finite number of cells in the computational domain will eventually lead to closed groups of cells of the period same as the number of cells in the group. The periodic cells represent invariant sets, which can be periodic motion and stable attractors of dynamical systems, and which represent the Pareto set in the context of MOPs. The rest of the cells form the domains of attraction of the invariant sets. For more discussions on the cell mapping methods, their properties and computational algorithms, the reader is referred to the book by Hsu [25].

2.4 Numerical Example

Consider the minimization of the vector function $\mathbf{F} = [f_1(\mathbf{k}), f_2(\mathbf{k})]$ such that f_1 and f_2 are given by,

$$f_1(\mathbf{k}) = k_1^2 + k_2^2 \tag{2.7}$$

$$f_2(\mathbf{k}) = (k_1 - 10)^2 + k_2^2, \tag{2.8}$$

where, $\mathbf{k} \in Q$ is a 2-dimensional vector of design parameters. The domain Q is expressed by box constraints:

$$Q = \{\mathbf{k} \in [-1, 10] \times [-1, 10] \subset \mathbf{R}^2\}, \tag{2.9}$$

The Pareto set and front returned by the NSGA-II are shown in Figures 2.1 and 2.2, respectively. It can be noticed that the population size affects the solution of the NSGA-II, and so is the number of generation. As a matter of fact, there is no definite relationship between the population size and the number of the design parameters. According to the Matlab documentation, the population size can be set in different ways and the default population size is 15 times the number of variables. Also, the maximum number of generations should not exceed 200 × $nvars$.

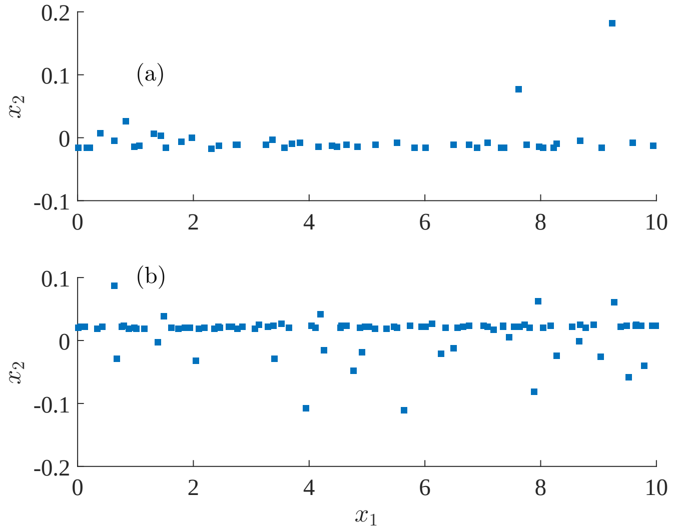

Figure 2.1: Pareto set: returned by NSGA-II: (a) $Npop$ =50 and $Ngens$ =200 , (b) $Npop$ =100 and $Ngens$ =200.

The solution set of the MOP algorithm based on the SCM for different cell divisions is shown in Figure 2.3. The corresponding Pareto front is depicted in Figure 2.4. As it is evident from Figure 2.3, the larger N values, the better the solution. Theoretically, SCM with $N = [\infty\ \infty]$ will produce the exact solution of this problem. However, it is clear that this is practically impossible because there is no infinite computer memory to handle this problem.

Though we are not concerned with the comparison between NSGA-II and SCM in this thesis, we can note that the SCM produces a well-distributed solution compared to that of the NSGA-II.

2.5 Summary

The NSGA-II and SCM for MOPs are detailed in this chapter. The first one is very popular in solving MOPs. The SCM is developed by our team and seems to produce very interesting results as we will see later. These two algorithms will be used in the next chapters to solve MOPs of a class of linear and nonlinear control problems.

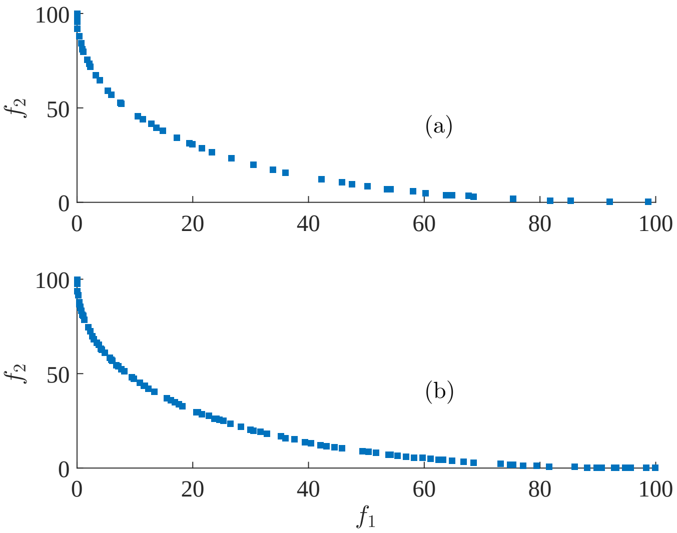

Figure 2.2: Pareto front corresponding to Figure 2.1 : (a) $Npop$ =50 and $Ngens$ =200 , (b) $Npop$ =100 and $Ngens$ =200.

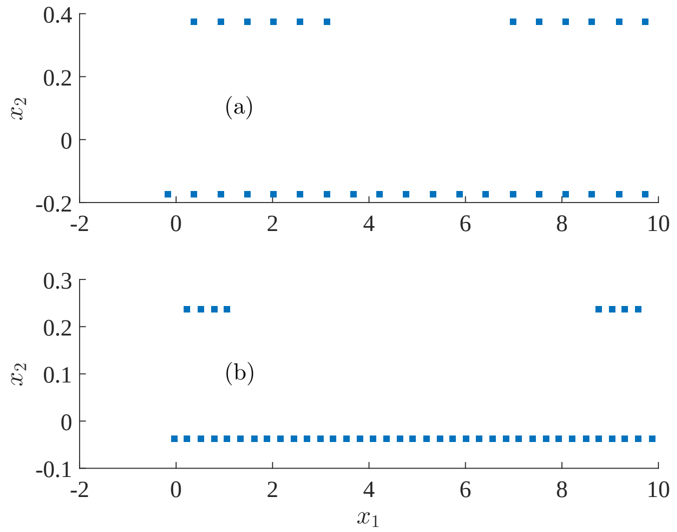

Figure 2.3: Pareto set: returned by SCM : (a) N =[20 20], (b) N =[40 40]

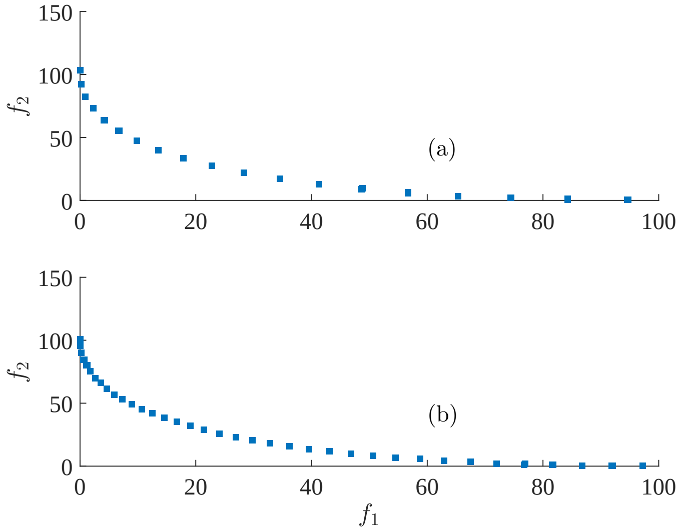

Figure 2.4: Pareto front corresponding to Figure 2.3: (a) N =[20 20], (b) N =[40 40]

Chapter 3

MANY-OBJECTIVE OPTIMAL AND ROBUST DESIGN OF PID CONTROLS WITH A STATE OBSERVER

3.1 Introduction

The proportional-integral-derivative (PID) control is the most used control algorithm. However, its tuning is not easy, especially when the design involves multiple conflicting design objectives. For instance, tuning the controller for small overshoot (M_p); low control energy; fast transient response (small peak time (t_p) or rise time (t_r)); and high rejection against measurement errors and noises is a very challenging task. It is well-known for control designer that a low control force is required to reduce the effect of the measurement noise and a large control force is needed for better noise rejection for the disturbance on the control signal. Furthermore, when an observer is used to estimate unmeasured states, high observer gains can cause a noise amplification. In linear control systems, the so-called Luenberger observer is usually used to estimate unavailable states from the available ones. Because the system is linear, the separation principle is used to design both of the controller and observer independently. The controller is designed first by the pole-placement method such that certain requirements on performance and/or robustness are satisfied. After that, the observer's gains are chosen so that some demands on accuracy and speed of response are met. In some textbooks, authors suggest a separation on the order of 2 to 10 between the desired closed-loop system's poles and the observer poles. This separation guarantees that the closed-loop performance dominates that of the estimator. This method of design can only handle specific requirements on both the controlled system and observer. However, other interesting results can be also found if the optimization of the controller's parameters and the observer gains is considered. The problem becomes more interesting when a many-objective optimization approach is used to find trade-offs between different non-agreeable design goals.

In this chapter, we study a many-objective optimal design of the PID control coupled with a linear observer, and make the following contributions: a) The gains of a PID control and an observer are designed simultaneously. Hence, the optimal design considers the stability robustness of both the control system and the estimator at the same time. b) We optimize the robustness to disturbance and measurement noises.

3.2 Linear Control System

Consider a linear control system

$$\begin{aligned}\dot{\mathbf{x}}(t) &= \mathbf{A}\mathbf{x}(t) + \mathbf{B}\mathbf{u}(t), \\ \mathbf{y}(t) &= \mathbf{C}\mathbf{x}(t),\end{aligned} \tag{3.1}$$

where $\mathbf{x} \in \mathbf{R}^n$, $\mathbf{u} \in \mathbf{R}^m$ and $\mathbf{y} \in \mathbf{R}^p$. Consider a full state feedback control $\mathbf{u} = -\mathbf{K}\mathbf{x}(t)$. The control gain $\mathbf{K}$ can be designed in a number of ways. When $(\mathbf{A}, \mathbf{B})$ is a controllable pair, we can design the control by the method of pole placement. If $(\mathbf{A}, \mathbf{C})$ is an observable pair, the following state estimator can be constructed:

$$\dot{\hat{\mathbf{x}}} = \mathbf{A}\hat{\mathbf{x}}(t) + \mathbf{B}\mathbf{u}(t) + \mathbf{L}(\mathbf{y}(t) - \mathbf{C}\hat{\mathbf{x}}(t)), \tag{3.2}$$

where $\hat{\mathbf{x}}$ is the estimate of $\mathbf{x}$ and $\mathbf{L}$ denotes the observer gain matrix. In this case, the actual control law is written as $\mathbf{u} = -\mathbf{K}\hat{\mathbf{x}}(t)$. The estimation error, $\mathbf{e} = \mathbf{x} - \hat{\mathbf{x}}$, satisfies the following equation,

$$\dot{\mathbf{e}}(t) = (\mathbf{A} - \mathbf{L}\mathbf{C})\mathbf{e}. \tag{3.3}$$

In linear control systems, the separation principle is used to design the controller and observer in two steps. In the first step, the poles of the closed-loop dynamic matrix, $\mathbf{A} - \mathbf{B}\mathbf{K}$, are placed in the desired locations so that the system performance meets the requirements. Then, the observer gain is designed so that observer dynamics are faster than those of the closed-loop system. To this end, a separation on the order of 2 to 10 is usually maintained between the poles of the matrix $\mathbf{A} - \mathbf{B}\mathbf{K}$ and those of $\mathbf{A} - \mathbf{L}\mathbf{C}$ [79]. In this chapter, we propose to design the gains of the PID control and the observer in a many-objective optimization setting.

In the following, we consider a second order oscillator as an example.

$$\begin{aligned}\dot{\mathbf{x}}(t) &= \begin{bmatrix} 0 & 1 \\ \omega_n^2 & 2\zeta\omega_n \end{bmatrix} \mathbf{x}(t) + \begin{bmatrix} 0 \\ \omega_n^2 \end{bmatrix} u(t), \\ y(t) &= [1\ 0]\ \mathbf{x}(t) = x_1(t),\end{aligned} \tag{3.4}$$

where $\omega_n = 5$, $\zeta = 0.01$.

Since the system is observable, a second-order estimator can be formulated as follow,

$$\dot{\hat{\mathbf{x}}} = \begin{bmatrix} 0 & 1 \\ \omega_n^2 & 2\zeta\omega_n \end{bmatrix} \hat{\mathbf{x}}(t) + \begin{bmatrix} 0 \\ \omega_n^2 \end{bmatrix} u(t) + \begin{bmatrix} l_1 \\ l_2 \end{bmatrix} (x_1(t) - \hat{x}_1(t)), \tag{3.5}$$

and the PID control is given by,

$$u(t) = k_p e_1(t) - k_d \hat{x}_2(t)) + k_i x_3, \tag{3.6}$$

where $e_1(t) = r(t) - \hat{x}_1(t)$, $r(t)$ is a step input, k_p, k_i and k_d are the gains and x_3 is the extended state with its first derivative given by $\dot{x}_3 = r - \hat{x}_1$. l_1 and l_2 are the observer parameters.

We consider the design vector $\mathbf{K} = [k_p, k_i, k_d, l_1, l_2]$ for the optimization problem. The design space, Q, for the parameters is chosen as follows,

$$Q = \{\mathbf{K} \in [10, 60] \times [1, 30] \times [1, 3] \times [1, 50000] \times [1, 50000] \subset \mathbf{R}^5\}, \tag{3.7}$$

The gains for the control and the observer are chosen such that the closed-loop matrices $\mathbf{A} - \mathbf{BK}$ and $\mathbf{A} - \mathbf{LC}$ are Hurwitz. Otherwise, the bounds of the design parameters are somewhat arbitrarily selected.

The many-objective optimal design problem is stated as,

$$\min_{\mathbf{K} \in Q} \{t_p, M_p, \|S(j\omega)\|_\infty, E_u, J_{IAE}, \mathbf{L}^T\mathbf{L}\}, \tag{3.8}$$

where t_p is the peak time, M_p is the maximum percentage overshoot, $\|S(j\omega)\|_\infty$ describes the disturbance rejection capability of the closed-loop system, where $S(j\omega)$ represents the transfer function from the disturbance to the closed-loop system output. $\|S(j\omega)\|_\infty$ is given by

$$\|S(j\omega)\|_\infty = \sup_{\omega \in \mathbb{R}} \sigma(S(j\omega)), \tag{3.9}$$

where σ is the largest singular value of the transfer function. To have a good disturbance rejection and reference signal tracking, the inequality, $\|S(j\omega)\|_\infty << 1$, must hold.

The last three objectives in Equation (3.8) are the control energy, E_u given by Equation(3.10), integral absolute error, J_{IAE} as defined Equation (3.11), and the Frobenius norm, $\mathbf{L}^T\mathbf{L}$, of the estimator gain matrix where $\mathbf{L} = [l_1, l_2]^T$.

$$E_u = \int_0^t u^T(\tau)u(\tau)d\tau \tag{3.10}$$

$$J_{IAE} = \int_0^t |e(t)|dt. \tag{3.11}$$

We also impose the constraints: $M_p \leq 10\%$, $\max(\lambda_r(\mathbf{A} - \mathbf{BK})) \leq -1$, and $\max(\lambda_r(\mathbf{A} - \mathbf{LC})) < \min(\lambda_r(\mathbf{A} - \mathbf{BK}))$. λ_r denotes the real parts of the matrix. The second constraint improves the relative stability and provides a certain stability robustness. The last condition to guarantee that the observer response is faster than that of the closed-loop system.

The solution of this optimization problem is defined via the concept of *dominancy* [1]. For this problem, we use the non-dominated sorting genetic algorithm

(NSGA-II) proposed in Section 2.2. Most of the default settings of this algorithm are kept and only two parameters are changed. They are population size and generation number. The population size is set to 150, and the number of generation is set to 800.

3.2.1 Numerical Results

The Pareto front, Pareto set, pole maps and selected system responses are discussed here. Figure 3.1 shows the Pareto set and Figure 3.2 shows some projections of the Pareto front. The Pareto set is colored with respect to the value of J_{IAE}. It can be seen from the Pareto set that a small tracking error is mainly associated with large k_p and k_i values, which indicates a large control effort.

The color in Figure 3.2 is also mapped to the value of J_{IAE}. The coloring adds a 3D visualization of the six dimensional Pareto front. The Pareto front shows a conflict relationship between t_p and M_p in Figure 3.2-a, between t_p and E_u in Figure 3.2-b, between $\|S(j\omega)\|_\infty$ and $\mathbf{L}^T\mathbf{L}$ in Figure 3.2-c, and finally between $\|S(j\omega)\|_\infty$ and E_u in Figure 3.2-d. These plots also demonstrate a non-agreeable relationship between E_u and J_{IAE} as indicated by the color in Figure 3.2-b, where the red denotes the highest value of J_{IAE}, and dark blue denotes the smallest value. These results are expected and have been reported in many books such as [79] and [14].

Figure 3.3-a shows the closed-loop poles of the matrix $\mathbf{A} - \mathbf{BK}$ and Figure 3.3-b portraits the eigenvalues of the matrix $\mathbf{A} - \mathbf{LC}$ on the Pareto set. It can be noticed that closed-loop poles are at least one unit further away from the left of the imaginary axis and the observer eigenvalues are to the left of those of the closed-loop system as imposed by the constraints.

The system responses at the worst $\max(\|S(j\omega)\|_\infty)$ and the best $\min(\|S(j\omega)\|_\infty)$ disturbance rejections are shown in Figures 3.4-a and 3.4-b, respectively, and those for the worse $(\max(\mathbf{L}^T\mathbf{L}))$ and best $((\min(\mathbf{L}^T\mathbf{L})))$ measurement noise rejection are depicted in Figures 3.4-c and 3.4-d. The external disturbance and measurement noise are modelled by white noises with the variance $\sigma^2 = 20$ and $\sigma^2 = 0.05$, respectively. Comparing the values of the absolute tracking error before (J_{IAE}) and after (J_{IAEd}) adding the disturbance, one can find out that the solution with the smallest $\|S(j\omega)\|_\infty$ has better rejection. However, measurement noise will be amplified because $\mathbf{L}^T\mathbf{L}$ will be large in this case as shown in Figure 3.4-c. In this figure, J_{IAE_n} denotes the absolute tracking error after adding the measurement noise. For low noise amplification, the solution with a small value of $\mathbf{L}^T\mathbf{L}$ must be selected. Finally, we point out that the user can choose any solution from the Pareto set that provides various compromises when meeting the performance requirements.

In the optimization we assume that the observer has zero error initially. The system responses under different initial estimation errors are reported in Figures 3.5-a and 3.5-c for a slow observer and in Figures 3.5-b and 3.5-d when the observer is fast. The simulation results exhibit that the initial conditions alter the transient response speed, overshoot and tracking error and in turn the total control effort. However, $\mathbf{L}^T\mathbf{L}$ and$\|S(j\omega)\|_\infty$ stay the same and they are insensitive to the initial estimation errors.

3.3 Concluding Remarks

We have studied the many-objective optimal PID control for a linear system with a state estimator. The optimization problem with 5 design parameters and 6 objective functions is solved by using the NSGA-II algorithm. Three performance and stability constraints have been imposed. The Pareto optimal designs form a set that offers a wide range of control compromises to meet the performance requirements. The numerical simulations have showed that the system has robust performance against external disturbances and measurement noise. It has been demonstrated that all the design objectives except $\|S(j\omega)\|_\infty$ and $\mathbf{L}^T\mathbf{L}$ are sensitive to the initial estimation errors.

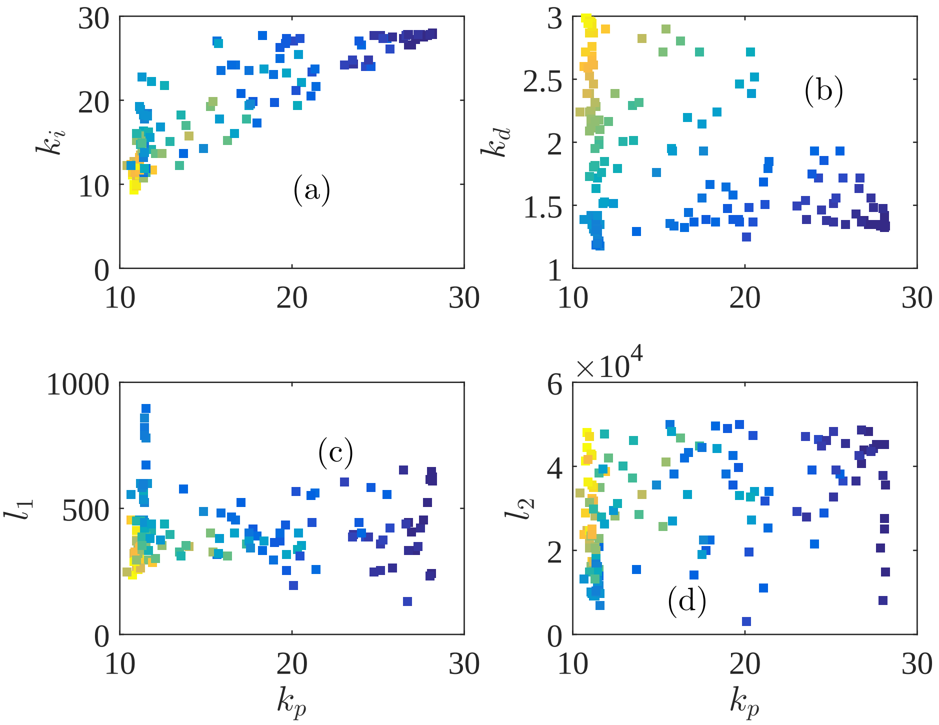

Figure 3.1: The Pareto set: (a) k_p versus k_i, (b) k_p versus k_d, (c) k_p versus l_1, (d) k_p versus l_2.The color code indicates the level of the objective function J_{IAE}. Red denotes the highest value, and dark blue denotes the smallest value.

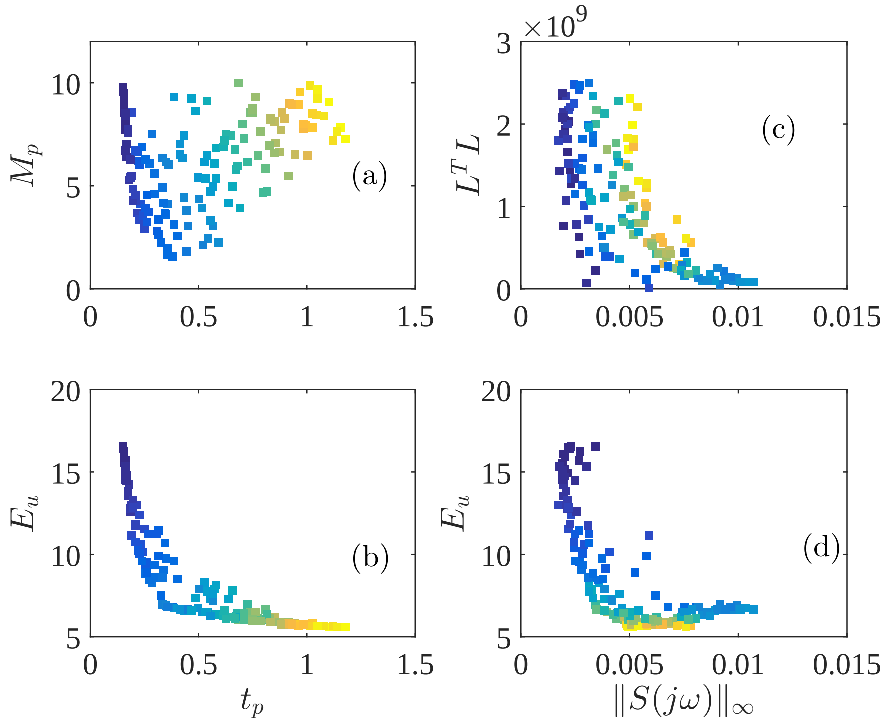

Figure 3.2: Projections of the Pareto front: (a) M_p versus t_p, (b) E_u versus t_p, (c) $\mathbf{L}^T\mathbf{L}$ versus $\|S(j\omega)\|_\infty$, (d) E_u versus $\|S(j\omega)\|_\infty$. The color code indicates the level of the objective function J_{IAE}. Red denotes the highest value, and dark blue denotes the smallest value.

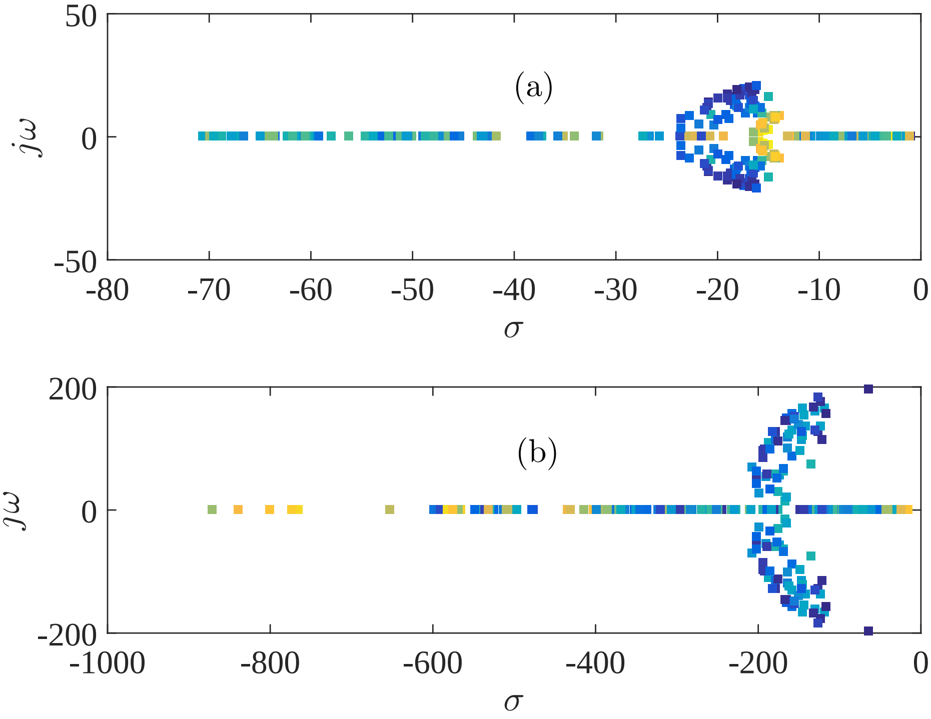

Figure 3.3: (a) The poles of the closed-loop system $\mathbf{A} - \mathbf{BK}$ corresponding to the Pareto set in Figure 3.1. (b) The estimator poles of the matrix $\mathbf{A} - \mathbf{LC}$. The color code indicates the level of the objective function J_{IAE}. Red denotes the highest value, and dark blue denotes the smallest value.

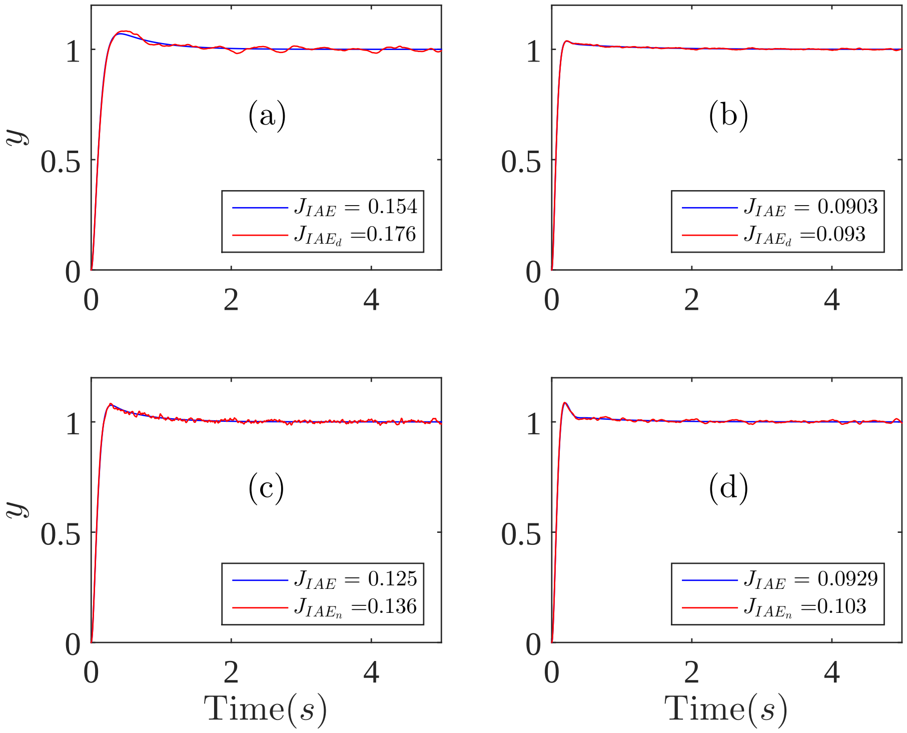

Figure 3.4: System responses before (blue solid line) and after (red solid line) adding an external disturbance (as in subplots a and b) or measurement noise (as in subplots c and d). (a) $\max(\|S(j\omega)\|_\infty)$, (b) $\min(\|S(j\omega)\|_\infty)$, (c) $\max(\mathbf{L}^T\mathbf{L})$, (d) $\min(\mathbf{L}^T\mathbf{L})$.

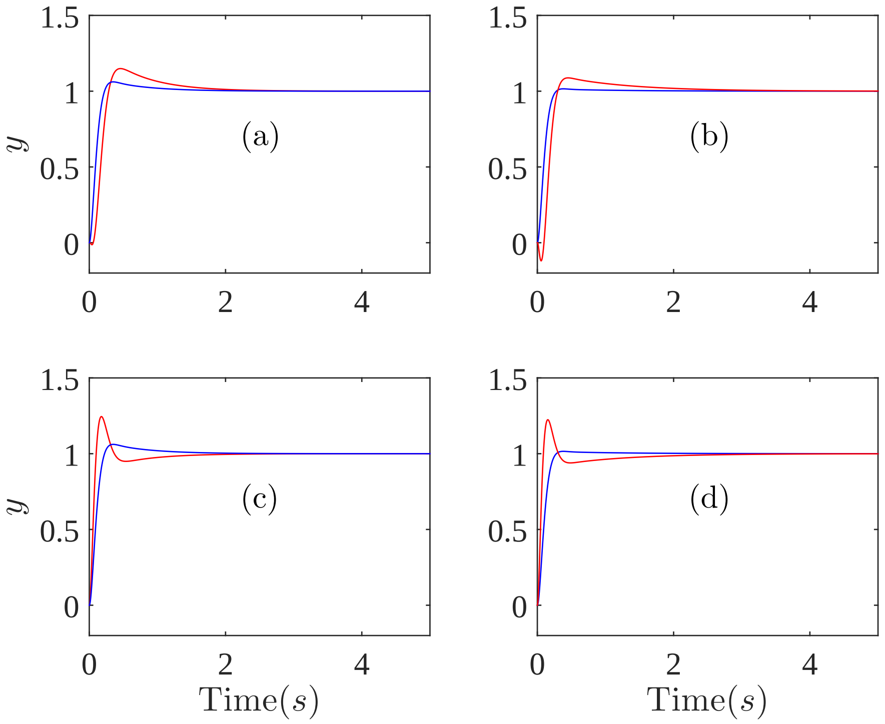

Figure 3.5: System responses with $\hat{\mathbf{x}}(0) = \mathbf{0}$ (blue solid line) and with $\hat{\mathbf{x}}(0) \neq \mathbf{0}$ (red solid line). (a) $\hat{\mathbf{x}}(0) = [-1\ -1]$ and the estimator is very slow, (b) $\hat{\mathbf{x}}(0) = [-1\ -1]$ and the estimator is very fast, (c) $\hat{\mathbf{x}}(0) = [1\ 1]$ and the estimator is very slow, (d) $\hat{\mathbf{x}}(0) = [1\ 1]$ and the estimator is very fast.

Chapter 4

MULTI-OBJECTIVE OPTIMAL CONTROL OF UNDER-ACTUATED BOGIE SYSTEM OF HIGH SPEED TRAINS

4.1 Introduction

Active controls of high speed trains have been receiving much attention because of their flexibility compared to passive technologies. The design of feedback controls must meet multiple and often conflicting requirements. In this chapter, we present a multi-objective optimization approach to design an active control system for a train subsystem called the bogie system.

With the development of active control technology, there is more and more literature on active control of railway vehicles in recent years. Much research is focused on railway vehicle ride comfort, the tilting train control and the secondary suspension semi-active or active control in order to improve the vehicle lateral and vertical smoothness, and to reduce high-frequency elastic vibration of the compartment body [80, 81]. Since the effect of bogie primary suspension on the critical velocity of railway vehicles has been well studied, researchers have proposed the use of semi-active and full-active suspension control to improve the lateral stability of the train [82–88]. There is a great variety of approaches for active primary suspensions. A list of configurations that have been studied and are suitable for implementation is provided in [87]. Active control may be applied in two different ways – directly or indirectly [89]. The direct control involves the application of an actuator on a solid wheelset or on an axle with independently rotating wheels. A practical compromise is to apply a yaw torque indirectly on the secondary suspension. This concept is called 'Secondary Yaw Control' (SYC). The actuators may be designed to replace the traditional passive yaw dampers so that active control of the running gear can be introduced without a substantial redesign of the bogie [90].

A single objective optimal design of feedback active controls for bogie systems using the linear-quadratic regulator (LQR) method have been discussed in [82, 91]. Therein, a performance index which includes the integral sum of the states and control energy is minimized through searching for the full-state feedback gains. In the design process, it is assumed that all the states are available for feedback, the controlled system is controllable and the external disturbances on the bogie wheelsets are known. However, assuming that all the states are measurable is expensive. Also, presuming that the noises affecting the wheelset motion are known and then using them as external inputs during the control design is an aggressive assumption. Usually in the control design, the system performance under disturbances and parametric variations is tested after the control is designed. To account for these uncertainties, the system sensitivity to disturbances and parameter variations as well as the relative lateral stability have to be taken into account in the design. In the active control design for trains, the lateral hunting stability of the vehicle at high speed is one of the most concerned dynamic problems. Loss of the vehicle lateral stability will cause poor ride comfort and even derail accidents. For these reasons, a robust and multi-objective optimal control design has to be considered, leading to a multi-objective optimization problem (MOP). For a robust and economic control system, the control effort or its Frobenius norm can be taken as an objective.

In this chapter, we solve the multi-objective optimal control design problem of the bogie system using the NSGA-II. In summary, we introduce the following contributions:

a. A MOO design of a feedback control for the bogie system by considering three objectives: the controlled system relative stability, disturbance rejection and the control energy consumption. To the best of our knowledge, such a control design for the bogie system is addressed for the first time in the literature.

b. Only two actuators are used to control the lateral displacements of the bogie frame and motors with four sensors mounted on the bogie frame to measure the frame lateral displacement, lateral velocity, yaw angle and its first time-derivative. With this hardware configuration, the system is not completely controllable and observable. As a result, the system is partitioned so that the controllable and observable part can be used to drive the internal modes to stability.

c. It is demonstrated that the Pareto optimal controls are insensitive to the variations of the train speed and wheel-rail contact conicity. These two quantities have huge impact on the bogie lateral stability [91].

4.2 The Bogie Model

In order to design the active control of the bogie, we consider a simplified model of this system as shown in Figure 4.1. The model describes the lateral movements of the bogie. We assume that the lateral position of the car body is predetermined. The lateral degrees of freedom of the bogie frame and driving system are taken into account in the model. Every bogie has two solid axle wheelsets which are attached to the bogie frame via suspension springs in the longitudinal and lateral directions. The drive systems which are suspended under the bogie frame are coupled to the bogie bodies via suspension springs and dampers in the sidelong direction. Each drive system exhibits lateral and yaw motions in the horizontal plane with respect to the bogie frame.

The dynamics of the bogie system is described by the following equation,

$$\mathbf{M}\ddot{\mathbf{X}} + \mathbf{C}\dot{\mathbf{X}} + \mathbf{K}\mathbf{X} = \mathbf{E}\mathbf{u}, \tag{4.1}$$

where $\mathbf{X} = [y_{w_1}, \varphi_{w_1}, y_{w_2}, \varphi_{w_2}, y_f, \varphi_f, y_{m_1}, y_{m_2}]^T$ and $\mathbf{u} = [u_1, u_2]^T$. y_{w_1}, y_{w2}, y_f, y_{m_1}, and y_{m_2} are the lateral displacements of wheelset 1, wheelset 2, bogie frame, motor 1 and motor 2, respectively. φ_{w_1}, φ_{w2} , and φ_f represent the yaw angles of wheelset 1, wheelset 2, and the bogie frame. u_1 and u_2 are lateral control forces applied on the bogie frame. The matrices $\mathbf{M}$, $\mathbf{C}$, and $\mathbf{K}$ are the mass, damping and stiffness components of the system. $\mathbf{E}$ is the vector describing the influence of the controls on the system dynamics. These matrices and vectors are listed in Appendix A and the values and definitions of system parameters are listed in Table A.1 [91]. The asymmetric part of the stiffness matrix $\mathbf{K}$ involving terms like $-2f\eta$ and $\frac{2\lambda_e l_0 f_\zeta}{r_0}$ represents the wheel-rail interaction forces. This is based on a simplified linear model of the wheel-rail interaction, and behaves like proportional feedback, which is responsible for the hunting instability.

The state equation of the system can be written as

$$\begin{aligned} \dot{\mathbf{x}}(t) &= \mathbf{A}\mathbf{x}(t) + \mathbf{B}\mathbf{u}(t) + \mathbf{F}d(t), & (4.2)\\ \mathbf{y} &= \mathbf{C}\mathbf{x}(t), & (4.3) \end{aligned}$$

where $d(t)$ is the external disturbance such as track irregularities applied on the wheelsets. The state vector is defined as

$$\begin{aligned} \mathbf{x} = [&y_{w_1}, \varphi_{w_1}, y_{w_2}, \varphi_{w_2}, y_f, \varphi_f, y_{m_1}, y_{m_2},\\ &\dot{y}_{w_1}, \dot{\varphi}_{w_1}, \dot{y}_{w_2}, \dot{\varphi}_{w_2}, \dot{y}_f, \dot{\varphi}_f, \dot{y}_{m_1}, \dot{y}_{m_2}]^T. \end{aligned} \tag{4.4}$$

The system matrices $\mathbf{A}$, and $\mathbf{B}$ and the vector $\mathbf{F}$ are given by,

$$\begin{aligned} \mathbf{A} &= \begin{bmatrix} \mathbf{0}_{8\times 8} & \mathbf{I}_{8\times 8} \\ -\mathbf{M}^{-1}\mathbf{K} & -\mathbf{M}^{-1}\mathbf{C} \end{bmatrix},\\ \mathbf{B} &= \begin{bmatrix} \mathbf{0}_{8\times 2} \\ \mathbf{M}^{-1}\mathbf{E} \end{bmatrix}, \quad \mathbf{F} = \begin{bmatrix} \mathbf{0}_{8\times 1} \\ \mathbf{M}^{-1}\mathbf{W} \end{bmatrix}, \end{aligned} \tag{4.5}$$

where the vector $\mathbf{W}$ is defined as

$$\mathbf{W} = [k_{py}, 0, k_{py}, 0, 0, 0, 0, 0]^T. \tag{4.6}$$

It can be shown that the system is not controllable and not observable. For the purpose of control design, we re-arrange the order of state variables in Equation (4.2) as follows,

$$\begin{aligned} \mathbf{x}_N = [&y_f, \varphi_f, \dot{y}_f, \dot{\varphi}_f, y_{w_1}, \varphi_{w_1}, y_{w_2}, \varphi_{w_2},\\ &y_{m_1}, y_{m_2}, \dot{y}_{w_1}, \dot{\varphi}_{w_1}, \dot{y}_{w_2}, \dot{\varphi}_{w_2}, \dot{y}_{m_1}, \dot{y}_{m_2}]^T. \end{aligned} \tag{4.7}$$

Let $\mathbf{T}$ be a matrix that transforms the state vector $\mathbf{x}$ into the new one such that $\mathbf{x}_N(t) = \mathbf{T}\mathbf{x}(t)$. The matrices and vectors of the transformed system are given by

$$\mathbf{A}_N = \mathbf{T}\mathbf{A}\mathbf{T}^{-1},\ \mathbf{B}_N = \mathbf{T}\mathbf{B}, \mathbf{F}_N = \mathbf{T}\mathbf{F}. \tag{4.8}$$

The transformed state equation of the system reads

$$\begin{bmatrix} \dot{\mathbf{x}}_{N_{4\times1}}(t) \\ \dot{\mathbf{x}}_{N_{12\times1}}(t) \end{bmatrix} = \begin{bmatrix} \mathbf{A}_{N_{4\times4}} & \mathbf{A}_{N_{4\times12}} \\ \mathbf{A}_{N_{12\times4}} & \mathbf{A}_{N_{12\times12}} \end{bmatrix} \begin{bmatrix} \mathbf{x}_{N_{4\times1}}(t) \\ \mathbf{x}_{N_{12\times1}}(t) \end{bmatrix} + \begin{bmatrix} \mathbf{B}_{N_{4\times2}} \\ \mathbf{0}_{12\times2} \end{bmatrix} \mathbf{u}(t) + \begin{bmatrix} \mathbf{0}_{4\times1} \\ \mathbf{F}_{N_{12\times1}} \end{bmatrix} d(t), \tag{4.9}$$

$$\mathbf{y} = \begin{bmatrix} \mathbf{C}_{N_{4\times4}} & \mathbf{0}_{4\times12} \end{bmatrix} \begin{bmatrix} \mathbf{x}_{N_{4\times1}}(t) \\ \mathbf{x}_{N_{12\times1}}(t) \end{bmatrix}. \tag{4.10}$$

In this equation, it is obvious that the matrix $\mathbf{C}_{N_{4\times4}}$ is $\mathbf{I}_{4\times4}$ where $\mathbf{I}$ denotes the identity matrix. The subsystem defined by the following state and output equations,

$$\dot{\mathbf{x}}_{N_{4\times1}} = \mathbf{A}_{N_{4\times4}}\mathbf{x}_{N_{4\times1}}(t) + \mathbf{A}_{N_{4\times12}}\mathbf{x}_{N_{12\times1}}(t) + \mathbf{B}_{N_{4\times2}}\mathbf{u}(t), \tag{4.11}$$

$$\mathbf{y} = \mathbf{C}_{N_{4\times4}}\mathbf{x}_{N_{4\times1}}(t), \tag{4.12}$$

is controllable and observable while the term $\mathbf{A}_{N_{4\times12}}\mathbf{x}_{N_{12\times1}}(t)$ acts as a disturbance to this subsystem.

Consider a partial state feedback control $\mathbf{u} = -\mathbf{K}_{2\times4}\mathbf{x}_{N_{4\times1}}(t)$. Using this control law, the closed-loop dynamic matrix of the system reads

$$\mathbf{A}_{cl} = \mathbf{A}_N - \mathbf{B}_N \begin{bmatrix} \mathbf{K}_{2\times4} & \mathbf{0}_{2\times12} \end{bmatrix}. \tag{4.13}$$

We have found that when a control gain $\mathbf{K}_{2\times4}$ is selected to stabilize the subsystem (4.11), the overall closed-loop system $\mathbf{A}_{cl}$ is also stable. Hence, the system is stabilizable Nevertheless, the stability of the closed-loop system puts a constraint on the control design. In addition to the stability of the closed-loop system, the robustness of the system to the parametric variations and external noises, and energy efficiency of the controller should also be taken into account in the design. These requirements will be set up and defined in the next section.

4.3 Multi-objective Optimal Control Design

We consider the multi-objective optimal control design with the gain $\mathbf{k} = [K_1, K_2, ..., K_7, K_8]$ as design parameters for the system discussed in Section 4.2. The design space for the parameters is chosen as follows,

$$Q = \{\mathbf{k} \in \mathbf{R}^8 \mid 0 \leq K_{1,2,3.4,5,7} \leq 10^8,\ -8\times10^{12} \leq K_{6,8} \leq 0\}. \tag{4.14}$$

Note that

$$\mathbf{K}_{2\times4} = \begin{bmatrix} K_1, K_2, K_3, K_4 \\ K_5, K_6, K_7, K_8 \end{bmatrix}. \tag{4.15}$$

The multi-objective optimal design problem is stated as,

$$\min_{\mathbf{k}\in Q}\{\max(\lambda_r), \|S(j\omega)\|_\infty, \mathbf{K}_{2\times4}^T\mathbf{K}_{2\times4}\}, \tag{4.16}$$

where $\lambda_r = \text{real}(eig\ (\mathbf{A}_{cl}))$ are the real parts of eigenvalues of the matrix $\mathbf{A}_{cl}$ defined in Equation (4.13). $\|S(j\omega)\|_\infty$ describes the disturbance rejection capability of the closed-loop system as illustrated in Section 3.2.

The term $\mathbf{K}_{2\times4}^T\mathbf{K}_{2\times4}$ denotes the Frobenius norm of the gain matrix $\mathbf{K}_{2\times4}$. Since the control system is optimized for zero initial conditions, the control effort cannot be included directly in the objective function and its Frobenius norm is used instead. By minimizing this norm, the total control energy is also minimized.

We apply the NSGA-II algorithm to solve the MOP. The population size is set to 300, and the number of generation is set to 1500. The results of this optimization are discussed in the next section.

4.4 Numerical Results

Recently, the speed of trains witnesses striking increases. In China, for instance, CRH380A (CRH: China Railway High-speed) hit operational speed up to 486.1 *km/h* in 2010. Then CHR380BL broke the record again in 2011, with operational speeds up to 487.3 *km/h* on the Beijing–Shanghai High-Speed Railway (HSR) during a test run on January 10, 2011. When an active control system is designed for these vehicles, the speed of the train has to be taken into consideration.

To examine the effect of speed on the bogie motion under the active control, we design the multi-objective optimal controls at four different speeds: 200 *km/h*, 220 *km/h*, 350 *km/h* and 500 *km/h*. Before presenting the comparison studies of these controls, we first discuss the properties of the Pareto set and Pareto front. Let us take the control design at 350 *km/h* as an example.

4.4.1 Properties of Pareto Optimal Controls

The Pareto front, Pareto set, and dynamics of the system states versus time before and after applying the control are discussed here. Figures 4.2 and 4.3 show two projections of the Pareto set. Figure 4.4 shows the corresponding Pareto front. The color in this figure is mapped to the value of the objective $\max(\lambda_r)$. The Pareto front shows a conflicting relationship between $\|S(j\omega)\|_\infty$ and $\max(\lambda_r)$ where the latter is less than one. In this range, the third objective fluctuates between its minimum and maximum. When $\max(\lambda_r(\mathbf{A}_{cl})) > -1$, $\|S(j\omega)\|_\infty$ and $\mathbf{K}_{2\times4}^T\mathbf{K}_{2\times4}$ are small indicating better disturbance rejection and less control effort, but the relative stability is poor. At $\max(\lambda_r) = -2.5$, the control system's relative stability is high, but the disturbance rejection competence and the norm $\mathbf{K}_{2\times4}^T\mathbf{K}_{2\times4}$ are low.

Three points of interest are labeled in Figure 4.4. $\mathbf{P_1}$ marked in the figure has a coordinate consisting of the minimum of all three objective functions, and is thus an ideal point not on the Pareto front. $\mathbf{P_2}$ is a point on the Pareto front that is closest to $\mathbf{P_1}$. It is called the knee point. $\mathbf{P_3}$ is a point on the Pareto front that has the largest Euclidian distance from $\mathbf{P_1}$. Hence, it is far away from the ideal solution. These points illustrate the properties of the MOO design.

The Pareto set shows that the state-feedback gains are very large. This result is expected since a very large force is required to drive such a big system. This can be seen also in Figure 4.5 where large magnitudes of u_1 and u_2 are required to stabilize the bogie system when $d(t) = A(H(t) - H(t - T))$ with the amplitude $A = 50mm$ and $T = 0.001s$. $H(t)$ denotes the Heaviside function. $d(t)$ mimics an impulse disturbance. This disturbance is applied to the wheelsets. The gain in this case is $\mathbf{k} = [9.8377,\ 5.8565,\ 5.3573,\ 7.3632,\ 3.2938,\ -2.8595 \times 10^5,\ 4.6284,\ -1.5407 \times 10^5] \times 10^7$ corresponding to the knee point $\mathbf{P}_2$.

The open loop and closed loop response to the disturbance $d(t)$ are shown in Figures 4.6 to 4.9. It can be seen from the figures that the bogie is unstable without active controls at 350 km/h. However, the proposed control stabilizes the unstable states successfully. Initially, the magnitudes of all the responses are small and then they settle down to zero. The lateral displacements of the motors and frame are between 0.0325 and 8.224 μm. The wheelset lateral displacements are in the range of -0.4-2.5 mm. The yaw angles of the frame body and the wheelsets are also small as shown in the figures.

The main concern in designing an active control of high speed trains is their lateral stability which changes with the speed of the train v and wheel-rail contact conicity λ_e, as shown in Figures 4.10 and 4.11, respectively. The wheel conicity increases with time due to wear which results in a considerable reduction in the train lateral stability and in some cases it can cause a derailment. To test the stability of the train, we changed v from 50 to 800 km/h and λ_e from 0.15 to 0.3. The test is conducted with four control designs. Two designs correspond to points $\mathbf{P}_2$ and $\mathbf{P}_3$ on the Pareto front. The other two designs represent the best relative stability $\min(\max(\lambda_r))$, and the worst relative stability $\max(\max(\lambda_r))$. The results show that the controlled system is insensitive to the train speed v and wheel-rail contact conicity λ_e. The control design with $\max(\max(\lambda_r))$ is very close to instability region, while the design with $\min(\max(\lambda_r))$ is highly stable. For the knee point $\mathbf{P}_2$, the maximum real part of the eigenvalues of the closed loop dynamic matrix $\mathbf{A}_{cl}$ is almost -2, while that for $\mathbf{P_3}$ is at -1, which still indicates a very good relative stability. The knee point may be more attractive to the engineers since it is the closest solution to the ideal one, although they have many options from the Pareto set.

4.4.2 Effect of Train Speed

Recall that we have obtained the Pareto optimal control designs at four different speeds: 200 km/h, 220km/h, 350 km/h and 500 km/h. From each Pareto set, we choose the control gains corresponding to the knee point. Figure 4.12 shows the train relative stability $\max(\lambda_r)$ as the function of the train speed for the control systems designed at the four different speeds. The results indicate that the Pareto optimal controls designed at various speeds are quite robust to the variations of the train speed.

The other two design objectives $(\|S(j\omega)\|_\infty, \mathbf{K}_{2\times4}^T\mathbf{K}_{2\times4})$ are $(0.0700, 3.1707e+24)$, $(0.0698, 2.5949e+24)$, $(0.0662, 4.2340e+24)$, $(0.0760, 1.0550e+25)$ for $v = 200$, 220, 350 and 500 km/h, respectively. Although the relative stability suggests that the design at lower speed is better, the other two objectives clearly indicate that the knee point of the Pareto front for v =350 km/h represents the best compromise. We should point out that the knee point is one of many design options in the Pareto set.

4.5 Concluding Remarks

We have studied the multi-objective optimal design of a partial state feedback control for an under-actuated high speed train bogie system. The control takes four measurements of the motion of the bogie frame, i.e. the lateral displacement and yaw angle and their first derivatives, and two lateral forces to stabilize the system. The MOP with 8 design parameters and 3 objective functions is solved with the NSGA-II algorithm. The Pareto set includes multiple design options, from which the user can choose to implement. Numerical simulations have been carried out. We have found that the Pareto optimal controls can stabilize the bogie system, and are robust against the system uncertainties, disturbances and variations of train speed.

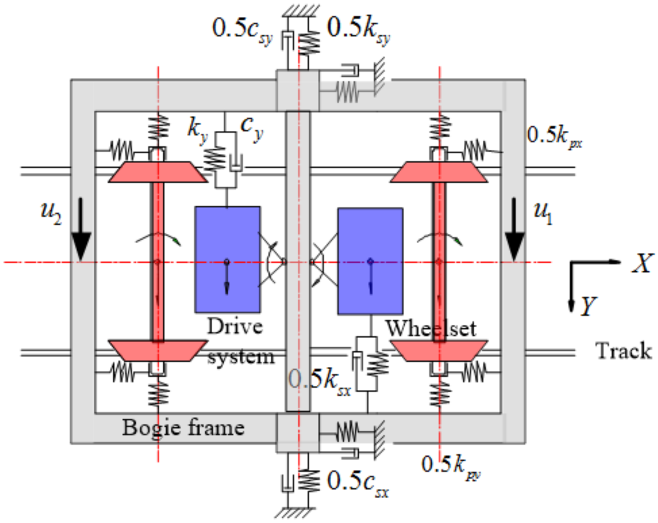

Figure 4.1: The model of the bogie with frame vibration controls.

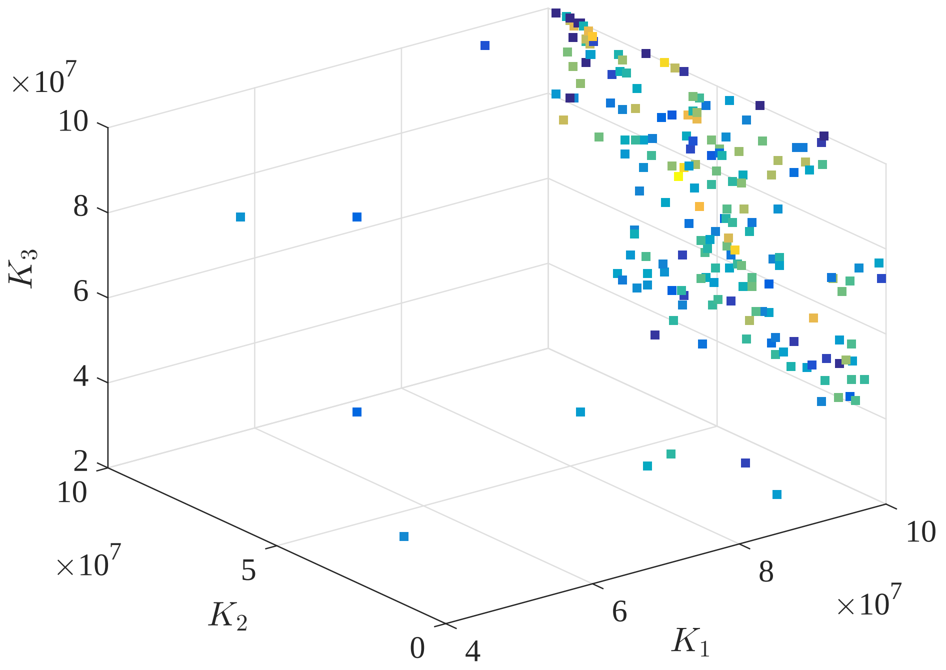

Figure 4.2: Projection #1 of the Pareto set when the train speed is v =350 km/h. The color code indicates the value of K_4. Red denotes the highest value, and dark blue denotes the smallest value.

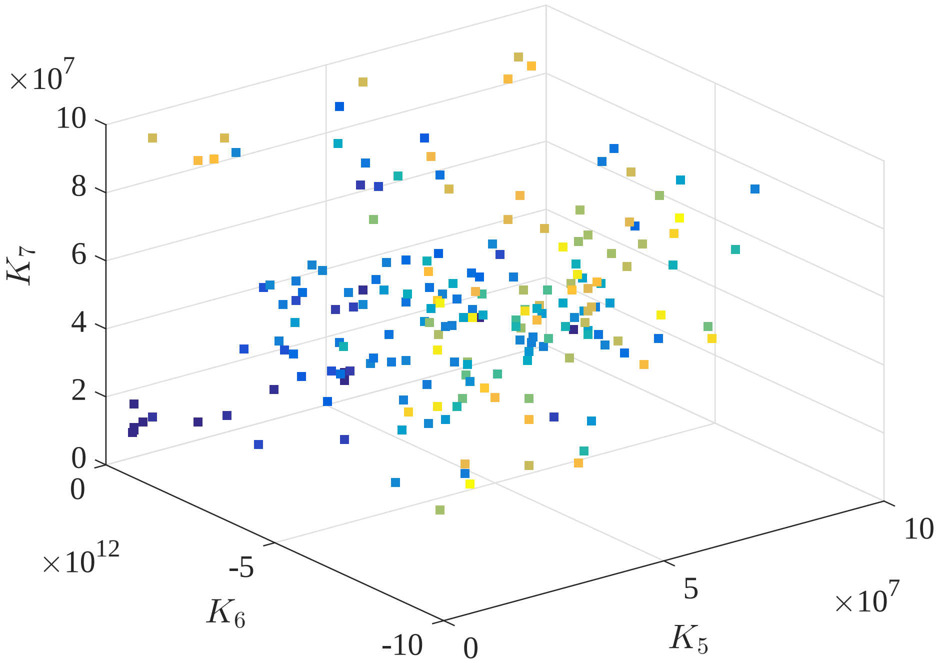

Figure 4.3: Projection #2 of the Pareto set when the train speed is v =350 km/h. The color code indicates the value of K_8. Red denotes the highest value, and dark blue denotes the smallest value.

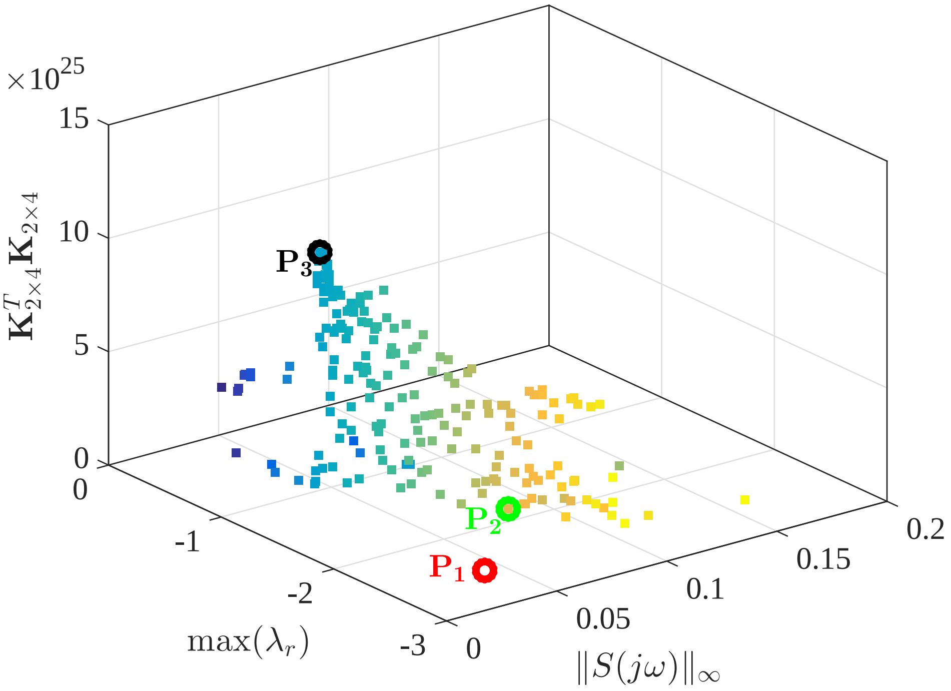

Figure 4.4: 3D visualization of the Pareto front when the train speed is v =350 km/h. The color code indicates the value of the objective function $\max(\lambda_r)$. Red denotes the highest value, and dark blue denotes the smallest value. $\mathbf{P}_1$, $\mathbf{P}_2$, and $\mathbf{P}_3$ are the ideal, knee, and far point, respectively.

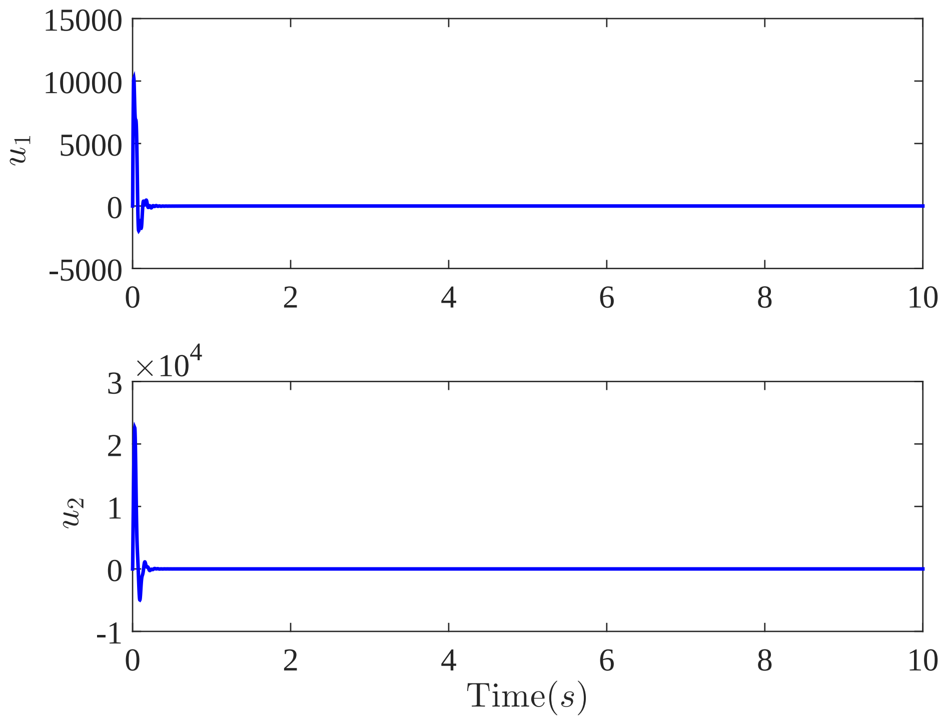

Figure 4.5: Lateral control forces when the train speed is v =350 km/h: (a) u_1 versus time, (b) u_2 versus time.

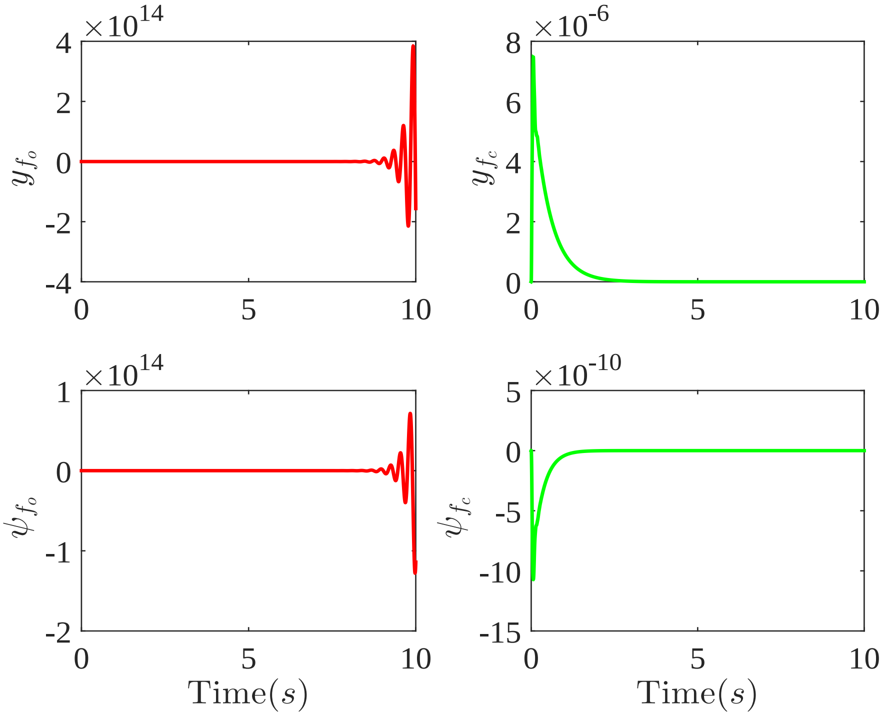

Figure 4.6: Open loop (y_{f_o}, ψ_{f_o}) and closed loop (y_{f_c}, ψ_{f_c}) dynamics of the bogie frame lateral displacement and yaw angle under the control corresponding to $\mathbf{P}_1$ when train speed is v =350 km/h.

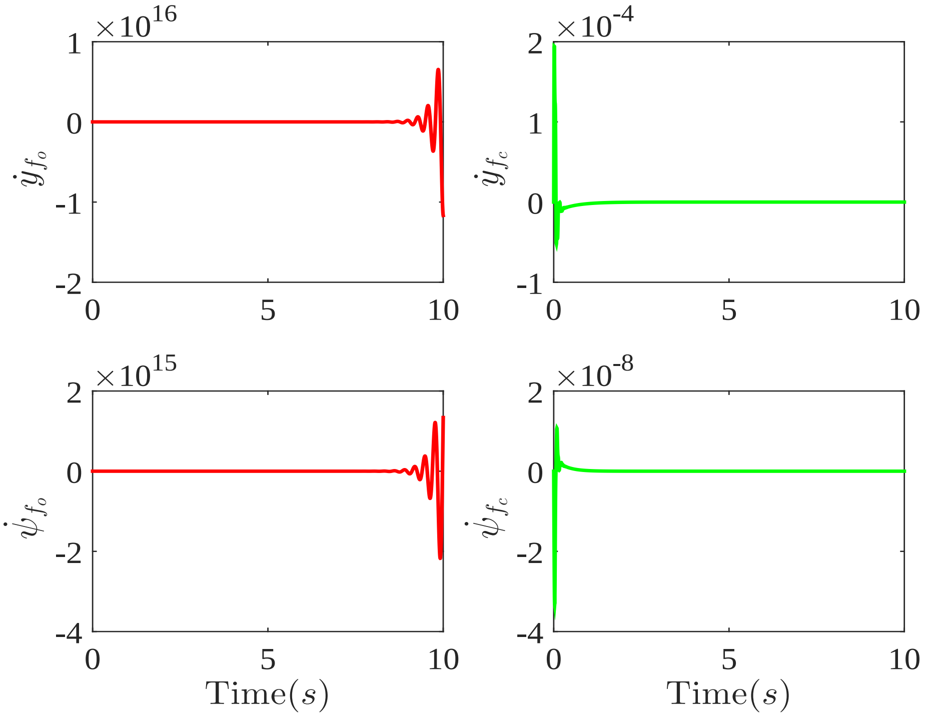

Figure 4.7: Open loop $(\dot{y}_{f_o}, \dot{\psi}_{f_o})$ and closed loop $(\dot{y}_{f_c}, \dot{\psi}_{f_c})$ dynamics of the bogie frame lateral velocity and yaw angle first-derivative under the control corresponding to $\mathbf{P}_1$ when train speed is v =350 km/h.

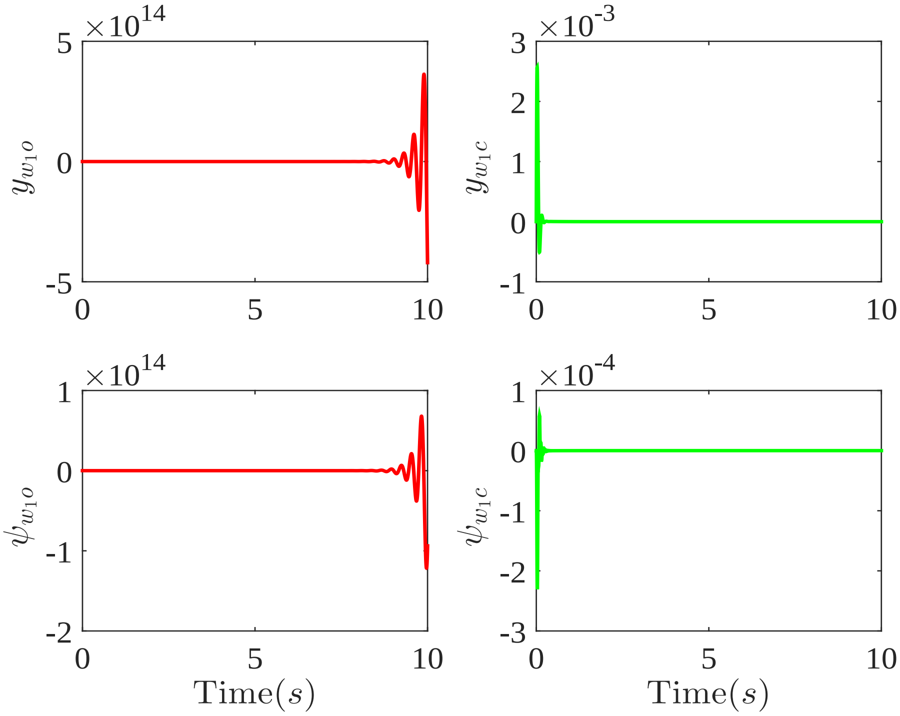

Figure 4.8: Open loop (y_{w1o}, ψ_{w1o}) and closed loop (y_{w1c}, ψ_{w1c}) dynamics of the bogie wheel 1 lateral displacement and yaw angle under the control corresponding to $\mathbf{P}_1$ when train speed is v =350 km/h.

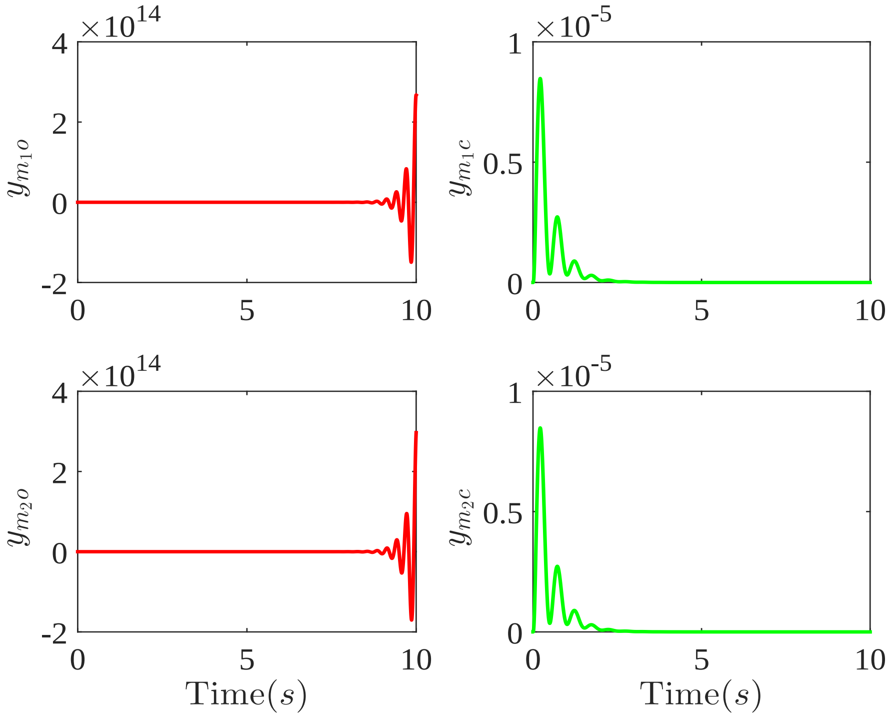

Figure 4.9: Open loop (y_{m1o}, y_{m2o}) and closed loop (y_{m1c}, y_{m2c}) dynamics of the bogie motor 1 and motor 2 lateral displacements under the control corresponding to $\mathbf{P}_1$ when train speed is v =350 km/h.

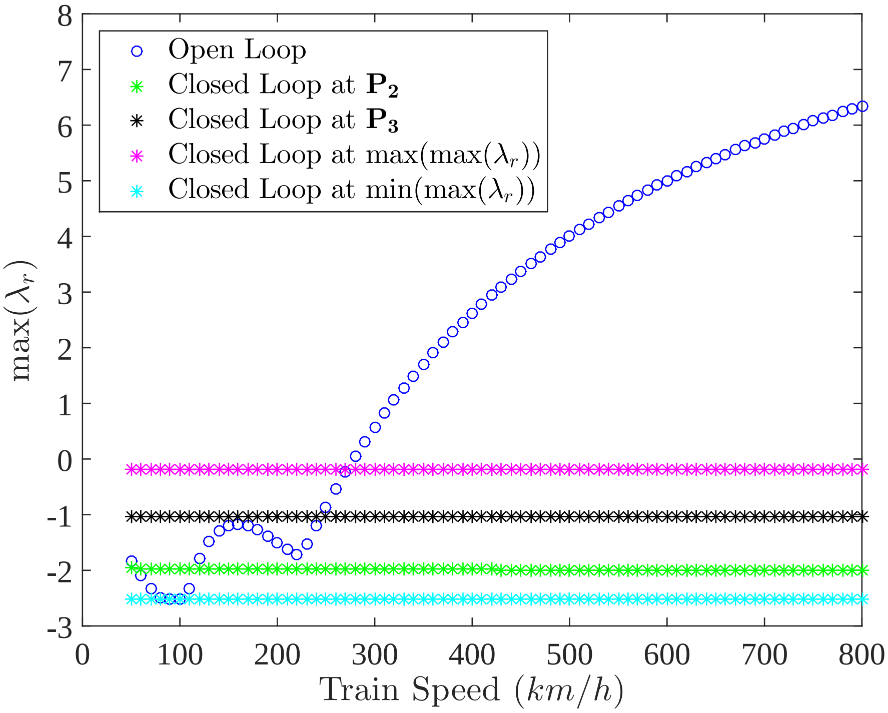

Figure 4.10: Open loop and closed-loop sensitivity to the train speed for the control designed at $v =$350 km/h.

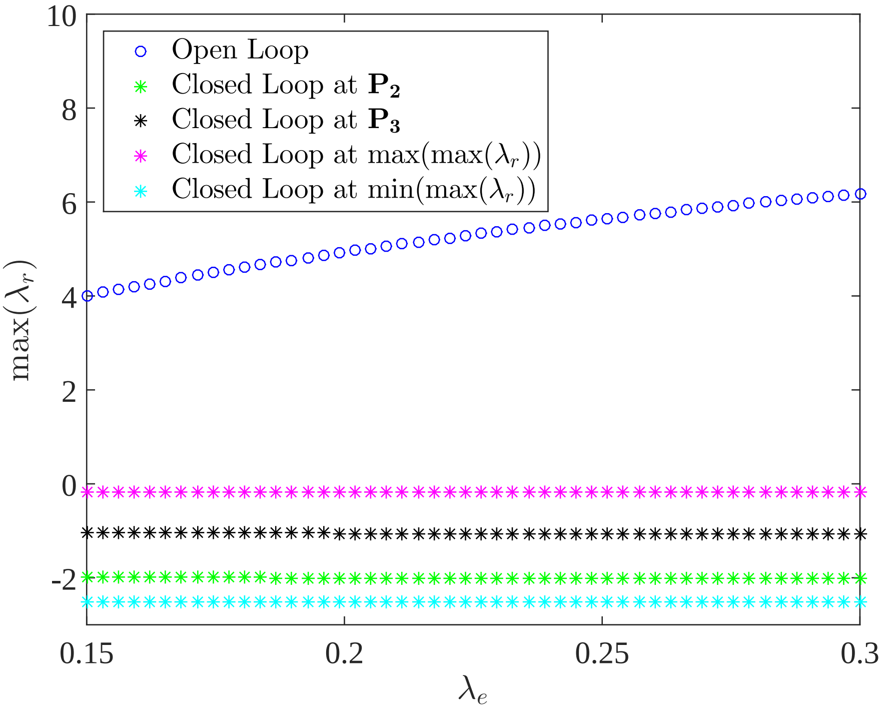

Figure 4.11: Open loop and closed-loop sensitivity to the wheel–rail contact conicity, λ_e, for the control designed at v =350 km/h.

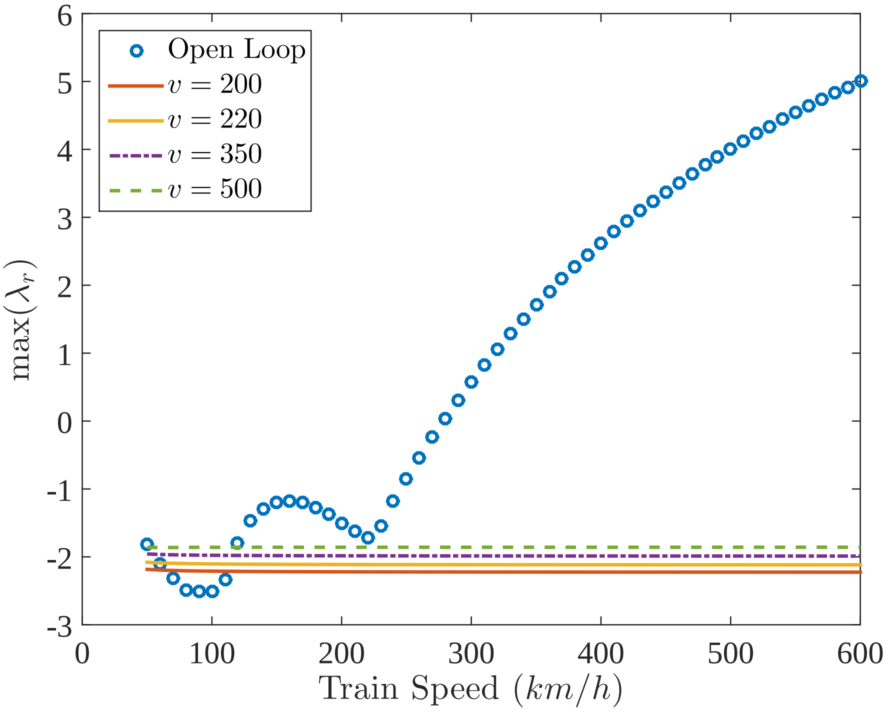

Figure 4.12: Variation of the relative stability $max(\lambda_r)$ with the train speed v for the control corresponding to the knee point of the Pareto front from the MOO designs at different speeds. The other two design objectives $(\|S(j\omega)\|_\infty, \mathbf{K}_{2\times4}^T\mathbf{K}_{2\times4})$ are $(0.0700, 3.1707e+24)$, $(0.0698, 2.5949e+24)$, $(0.0662, 4.2340e+24)$, $(0.0760, 1.0550e+25)$ for $v = 200$, 220, 350 and 500 km/h, respectively.

Chapter 5

MANY-OBJECTIVE OPTIMAL DESIGN OF SLIDING MODE CONTROLS

5.1 Introduction

The history of the variable structure control such as the sliding mode control (SMC) can be traced back to the 1950s when it was first proposed by Emelyanov and several co-authors in the former Soviet Union [92]. Because feedback controls are usually designed to achieve multiple and often conflicting performance goals, extensive investigations are needed to tune control parameters in order to obtain the best performance [58]. In this chapter, we present a many-objective optimization approach for the quantitative design of SMCs with parameter adaptation.

The SMC is interesting because it has, to a certain extent, a robust behavior to parametric uncertainties and external noises. This property comes from the fact that the SMC implements a switching term which steers the state trajectories to a predefined stable manifold known as the sliding surface. When the state trajectories hit the surface, they stay on it forever [93]. The SMC can reach the sliding surface in a finite time and achieve a very good tracking accuracy [94]. To achieve robustness, one usually applies a discontinuous switching term and high feedback gain. However, this leads to high frequency switching effect or what is called chattering. The chattering is undesirable and detrimental because it may cause instability through triggering high-frequency unmodeled dynamics of the system. To avoid high-frequency chattering, the boundary layer technique is usually used but at the expense of the robustness [94]. That is to say, when the SMC is implemented in real-life applications, the robustness is traded-off for the reduction in the control system chattering.

The adaptive control can use the response history to estimate constant or slowly time-varying parameters of the system. When the time-varying disturbances are present as in many practical systems, the transient response of the controlled system becomes unpredictable. To overcome this difficulty, an adaptive sliding mode control (ASMC) was suggested in [95]. This ASMC can resist uncertainties and learn from the system prior information. Another ASMC that combines the adaptivity provided by learning algorithms and the robustness of the SMC was presented in [96]. It was also applied in many applications such as non-affine nonlinear vehicle systems

[97], fault tolerant flight control systems [98], guidance of a homing missiles [99], the roll-coupled maneuvers of aircrafts [100], fault tolerant control for flexible spacecrafts [101], speed drives [102], manipulators [103], and mechanical servo systems with LuGre friction compensation [104]. However, these controllers were designed by considering a single objective, usually minimizing the tracking error.

In the design of the ASMC, one has to make trade-offs among several conflicting objectives such as the performance, robustness, and control effort [105]. The system performance can be measured by many indices such as the peak time, rise time, settling time, overshoot and tracking error in the time domain, or crossover frequency, phase margin and gain margin in the frequency domain. The system robustness includes stability robustness and disturbance rejection robustness.

In this study, we study a many-objective optimal (MOO) design of the ASMC and we make the following contributions:

1. A MOO design of the ASMC by considering four design objectives: the rise time t_r, disturbance rejection efficiency $\|S(j\omega)\|_\infty$, control energy consumption E_u, and tracking integral absolute error J_{IAE}.

2. An enhancement of the ASMC ability to reject external noises by including the objective $\|S(j\omega)\|_\infty$ as one of the design criteria. Furthermore, the stability robustness is also improved by pushing the poles of the linearized closed-loop system away from the imaginary axis. These two design criteria have been always assumed to be guaranteed when the ASMC is implemented, but never included explicitly in the design to tune the control parameters.

3. A new post-processing algorithm that guides the decision-maker to choose control designs with the best trade-offs among the different options in the Pareto set.

5.2 Adaptive Sliding Mode Control

Uncertainties in the system dynamics and unwanted disturbances are unavoidable. They are usually difficult to model. In this work, we use a double integrator system with uncertainties as an example to demonstrate the design of many-objective optimal ASMCs. Consider

$$\begin{aligned} \dot{x}_1 &= x_2 \\ \dot{x}_2 &= f_1\left(x_1, x_2\right) + a f_2\left(x_1, x_2\right) + g\left(x_1, x_2\right) u(t) + d(t), \end{aligned} \tag{5.1}$$

and the output of the system reads

$$y = h(x_1, x_2), \tag{5.2}$$

where f_1, f_2 and g are nonlinear functions of their arguments. We assume that $g(x_1, x_2) \neq 0$ and a is one of the parameters of the system model to be estimated. We also assume that a is either constant or slowly time-varying parameter, and that it is the only parameter to be estimated. $u(t)$ denotes the control force. $d(t)$ is an unknown external disturbance. h is a linear function of its arguments. In this study, we consider the ASMC because of its robustness in the presence of parametric uncertainties and external disturbances and its ability to online estimate system parameters. We assume that $y = x_1$. The control law can be derived by first constructing a sliding surface s as follows:

$$s = \dot{e} + ce, \quad c > 0, \tag{5.3}$$

where $e = x_1 - x_d$ and $\dot{e} = x_2 - \dot{x}_d$. x_d and $\dot{x}_d$ represent the desired tracking signal and its derivative, respectively. To derive the nominal control $u_n(t)$, we set $\dot{s} = 0$ where $\dot{s}$ reads,

$$\begin{aligned} \dot{s} &= \ddot{e} + c\dot{e} = \dot{x}_2 - \ddot{x}_d + c\dot{e} \\ &= f(x_1, x_2) + af_2(x_1, x_2) + g(x_1, x_2)\, u_n(t) - \ddot{x}_d + c\dot{e}. \end{aligned} \tag{5.4}$$

The nominal control force is given by,

$$u_n(t) = 1/g(x_1, x_2) \left\{ -f(x_1, x_2) - af_2(x_1, x_2) + \ddot{x}_d - c\dot{e} \right\}. \tag{5.5}$$

We note that $d(t)$ is not included in the nominal control because it is unknown. The total control $u(t)$ of the ASMC consists of the nominal control $u_n(t)$, and a discontinuous switching term. The discontinuous term depends on the choice of the reaching law which describes how the system trajectory reaches the predefined sliding surface. Here, we choose the constant rate reaching law given by,

$$\dot{s} = -\eta \times sign(s), \quad \eta > 0, \tag{5.6}$$

where $sign(s)$ is the signum function. With this choice of the reaching law, the total control law takes the following form,

$$u(t) = 1/g(x_1, x_2) \left\{ -f(x_1, x_2) - \hat{a}f_2(x_1, x_2) + \ddot{x}_d - c\dot{e} - \eta \times sign(s) \right\}. \tag{5.7}$$

where $\hat{a}$ is the estimate of a. The adaptation law to estimate the parameter a can be derived subsequently. Consider a positive definite Lyapunov function,

$$V = \frac{1}{2}s^2 + \frac{1}{2\gamma}\tilde{a}^2, \quad \gamma > 0, \tag{5.8}$$

where the estimation error $\tilde{a}$ is given by

$$\tilde{a} = \hat{a} - a, \quad \dot{\tilde{a}} = \dot{\hat{a}}. \tag{5.9}$$

Taking the time derivative of Equation (5.8), we get

$$\dot{V} = s\dot{s} + \frac{1}{\gamma}\tilde{a}\dot{\hat{a}} = \tilde{a}(sf_2\left(x_1, x_2\right) + \frac{1}{\gamma}\dot{\hat{a}}) - \eta|s|. \tag{5.10}$$

The closed-loop system is asymptotically stable, i.e. $\dot{V} = -\eta|s| < 0$, if the adaptation control algorithm of $\dot{\hat{a}}$ is given by

$$\dot{\hat{a}} = -\gamma sf_2\left(x_1, x_2\right). \tag{5.11}$$

In this equation, γ is the adaptation gain. To avoid chattering caused by the switching term $sign(s)$, we replace it with $sat(s, \phi)$ where ϕ represents the width of the saturation layer.

$$sat(s, \phi) = \begin{cases} s/\phi, & if\ \ |s| \leq \phi \\ sign(s), & if\ \ |s| > \phi \end{cases} \tag{5.12}$$

The control law becomes

$$u(t) = 1/g\left(x_1, x_2\right)\left\{-f\left(x_1, x_2\right) - \hat{a}f_2\left(x_1, x_2\right) + \ddot{x}_d - c\dot{e} - \eta \times sat(s, \phi)\right\}. \tag{5.13}$$

The analytical design of the ASMC is now complete. Next, we consider the optimal selection of control gains and parameters c, η, ϕ, and γ to achieve the robustness against external noises and parameter uncertainties, and to meet the objectives of low control energy, fast response and accurate tracking. As discussed previously, this task leads to a many-objective optimization problem.

Before we present the MOO design of the ASMC, we first prepare to deal with the design of the stability robustness and disturbance rejection robustness for nonlinear systems. To this end, the closed-loop system of Equation (5.1) is linearized around the sliding mode surface $s = 0$ when the system reaches the steady-state given by

$$\mathbf{x}_{ss} = [x_d, \dot{x}_d]^T. \tag{5.14}$$

The system linearized at the steady-state $\mathbf{x}_{ss}$ with a matched unknown external noise reads

$$\delta\dot{\mathbf{x}} = \mathbf{A}_{cl}\delta\mathbf{x} + \mathbf{B}_{cl}d(t). \tag{5.15}$$

The stability robustness of the nonlinear system is defined by the maximum real part of the eigenvalues of the closed-loop dynamic matrix, $\mathbf{A}_{cl}$ in the steady-state. The noise rejection robustness is measured by $\|S(j\omega)\|_\infty$, which represents the infinity norm of the transfer function between the system output δx_1 and the unknown input disturbance $d(t)$. We have omitted the detail expressions for $\mathbf{A}_{cl}$ and $\mathbf{B}_{cl}$ in this section. These expressions will be provided for the examples.

5.3 Many-objective Optimal Design

In the MOO design, we take $\mathbf{k} = [c, \eta, \gamma, \phi]$ as the design parameters. The MOP is stated as,

$$\min_{\mathbf{k}\in Q}\{t_r, \|S(j\omega)\|_\infty, E_u, J_{IAE}\}, \tag{5.16}$$

where t_r is the rise time when the system output $y = x_1$ takes to cross from the 10% to 90% of the step reference x_d. As we explained in Section 3.2, $\|S(j\omega)\|_\infty$ describes the disturbance rejection capability of the closed-loop system. The objectives E_u and J_{IAE} are the control energy given by Equation (3.10), and integral absolute error defined in Equation (3.11), respectively.

5.4 A Numerical Example

Consider a Duffing system with dry friction such that

$$\begin{aligned}\dot{x}_1 &= x_2, \\ \dot{x}_2 &= -p_1x_1 - px_2 - ax_2^2 \times sign(x_2) - p_2x_1^3 + u(t),\end{aligned} \tag{5.17}$$

and the output equation

$$y = x_1. \tag{5.18}$$

The coefficient of the dry friction coefficient a is to be estimated. The complete control law and the adaptation law are given by,

$$u(t) = p_1x_1 + px_2 + \hat{a}x_2^2 \times sign(x_2) + p_2x_1^3 + \ddot{x}_d - c\dot{e} - \eta \times sat(s, \phi), \tag{5.19}$$

$$\dot{\hat{a}} = -\gamma s x_2^2 \times sign(x_2). \tag{5.20}$$

The design space of the parameters $\mathbf{k} = [c, \eta, \gamma, \phi]$ is chosen as,

$$Q = \{\mathbf{k} \in \mathbf{R}^4 \mid 1 \leq c \leq 3,\ 0 \leq \eta \leq 10,\ 1 \leq \gamma \leq 100,\ 0.01 \leq \phi \leq 0.1\} \tag{5.21}$$

The solutions of the MOP in Equation (5.16) are searched with the help of time-domain responses generated by the Runge–Kutta fourth order algorithm. The time duration of the integrals in the objective functions is $0 \leq t \leq 5$ seconds. The integration time step is 0.001. We have taken the nominal values of the system parameters as $p_1 = -1.0$, $p = 0.25$, $p_2 = 1$ and $a = 2$.

We consider a unit step input as a reference signal in the design. So, the steady-state vector in Equation (5.14) is given by

$$\mathbf{x}_{ss} = [x_d, 0]^T \tag{5.22}$$

The closed-loop system matrices in Equation (5.15) read

$$\mathbf{A}_{cl} = \begin{bmatrix} 0 & 1 \\ -c\frac{\eta}{\phi} & -(\frac{\eta}{\phi} + c) \end{bmatrix}, \quad \mathbf{B}_{cl} = \begin{bmatrix} 0 \\ 1 \end{bmatrix}. \tag{5.23}$$

We impose a constraint for the stability robustness,

$$\max(\lambda_r(\mathbf{A}_{cl})) \leqslant -2, \tag{5.24}$$

where $\lambda_r(\mathbf{A}_{cl})$ denotes the real part of eigenvalues of the matrix $\mathbf{A}_{cl}$.

Searching for the optimal parameters of the ASMC in the MOP setting is a laborious task [106]. In this study, the NSGA-II algorithm is used to solve the MOP. The population size is set to 100, and the number of generation is set to 600.

Next, we discuss the results of this optimization problem. The Pareto front is shown in Figure 5.1. The color in the subplots a, c and d is mapped to the value of J_{IAE} while that of the subplot b denotes the value of $\|S(j\omega)\|_\infty$. The color is used to add a 3D visualization of the 4D Pareto front.

The Pareto front demonstrates a competing relationship between E_u and each of t_r, J_{IAE} , and $\|S(j\omega)\|_\infty$ [79]. The relationships between the other objectives may not clear because of the dimension of the objective space. However, conflicting nature can be recorded at specific regions. For instance, t_r and $\|S(j\omega)\|_\infty$ are competing when the latter is very small, that is $\|S(j\omega)\|_\infty \in [3.0 \times 10^{-4}, 3.5 \times 10^{-4}]$. As shown in Figure 5.2, in this region all the design parameters are large except the saturation layer ϕ is small. Beyond this region, an increase in t_r is associated with an increase in $\|S(j\omega)\|_\infty$ and J_{IAE}, with a reduction in the control effort, suggesting that the system tends to have a slower response, less noise rejection ability and less tracking accuracy when $\|S(j\omega)\|_\infty > 3.5 \times 10^{-4}$, but the control energy is reduced.

The Pareto set is shown in Figure 5.2. To show the corresponding design variables for each point in the Pareto front, the Pareto set is also colored with respect to J_{IAE} values. At the right up corner of the subplots a and b and at the right low corner of the subplot c of this figure, it can be observed that the tracking error indicated by the dark blue color is small which means, according to Figure 5.1-b, that a very high control effort is required to achieve that. The disturbance rejection and stability robustness are also very good in this region. Some of these findings can be explained by Equation (5.3). It can be noted that the larger the value of c, the smaller the magnitude of the tracking error. Also, by calculating the eigenvalues of the matrix $\mathbf{A}_{cl}$, it can be found that increasing the values of the parameters c and η or decreasing ϕ improves the system robustness. Similarly, the disturbance rejection ability goes up when c and η go up or ϕ goes down [107]. This can be confirmed by analytically calculating $\|S(j\omega)\|_\infty$ from Equation (5.15) with $\mathbf{A}_{cl}$ given in Equation (5.23). The parameter adaptation gain γ has an effect on the design objectives only during the transient stage.

The system responses are shown in Figure 5.3 with the extremum objectives including

1. The fastest speed response $\mathbf{k}$ = [0.7321, 0.0003, 113.1871, 0.4513],

2. The best disturbance rejection $\mathbf{k} = [0.7437, 0.0003, 162.5056, 0.4544]$,

3. The smallest energy expenditure $\mathbf{k} = [0.9945,\ 0.0009,\ 7.9028,\ 0.6912]$ and

4. The smallest tracking error $\mathbf{k} = [0.7328,\ 0.0004,\ 123.6633,\ 0.4508]$.

Each subplot of Figure 5.3 shows two curves of the system response before and after adding disturbance and 20% uncertainty in the system parameter. To test the disturbance rejection, we introduce a white noise with variance $\sigma_w^2 = 20$ to the system in the numerical simulation. We should point out that this is a very strong noise. In this figure, $J_{IAE_{du}}$ denotes the system tracking error after applying the uncertainty and disturbance. A slight increase in $J_{IAE_{du}}$ can be observed. It should be noted that $J_{IAE_{du}}$ in subplots a, b and d is the same as J_{IAE}. In general, the system performs well in the existence of the assumed uncertainty because the ASMC is designed such that the disturbance rejection and stability robustness are explicitly considered. The optimal values of $\|S(j\omega)\|_\infty$ fall between 3×10^{-4} and 9×10^{-4}, which indicates an excellent disturbance rejection ability. The real part of the largest eigenvalue of the steady-state linearized system is at least 2 units away from the imaginary axis as imposed by Equation (5.24). This provides an adequate stability margin for robustness.

5.5 A Post-Processing Algorithm

As we know, the solution of MOPs is a set of solutions. All the points on the Pareto front are equally important. Even though the decision-maker has the authority to pick up any solution from this set, the selection process is not easy. To facilitate this operation, we introduce an algorithm that operates on the Pareto front. The pseudo code of the algorithm is listed in Table 5.1. The algorithm starts by finding the ideal point made of the minimum values of all the objectives of the Pareto front. Then, the L^2-norm distance d between the ideal point and points on the Pareto front is calculated. The maximum distance $d_{\max}$ and the minimum distance $d_{\min}$ are found. The difference $d_{\max} - d_{\min}$ is divided by a pre-specified number $nDiv$ such that $h = (d_{\max} - d_{\min})/nDiv$. Circles centered at the ideal point with radii $r_i = d_{\min} + i * h$ for $i = 0, 2, .., nDiv$ are used to section the Pareto front and rank the control design by the radius r_i.

The post-processing algorithm is applied to the Pareto front in Figure 5.1 with $nDiv = 200$. Top 20% of the Pareto optimal designs are shown in Figures 5.4 and 5.5 with the objectives falling in the following range,

$$\begin{aligned} 0.7370 &\leq t_r \leq 0.7780, \\ 0.0004 &\leq \|S(j\omega)\|_\infty \leq 0.0005, \\ 36.6848 &\leq E_u \leq 66.2776, \\ 0.4999 &\leq J_{IAE} \leq 0.4599. \end{aligned} \tag{5.25}$$

The system responses before and after adding uncertainties and disturbances to the system are shown in Figure 5.6 for four randomly chosen designs. The system has very good closed-loop performances even in the existence of the parametric and dynamic uncertainties.

5.6 Conclusions

A many-objective optimal design of an adaptive sliding mode control applied to a second-order uncertain system is studied. The objectives include some of the most important properties of a control system such as maximizing the stability robustness and disturbance rejection ability, and minimizing the rise time, control energy and integrated absolute tracking error. The optimal control is shown to be truly robust with respect to model uncertainties and external disturbances in the numerical simulations. To facilitate users to choose the best trade-offs from the Pareto optimal designs, we have developed a post-processing algorithm. The numerical simulations show that the proposed many-objective optimization method and post-processing algorithm offer a novel alternative to quantitative design of nonlinear controls.

Table 5.1: Pseudo code of post-processing algorithm .

```
Program: Postprocessing_algorithm
Input: Pareto front $pf$, Pareto set $ps$,
       Number of divisions $nDiv$,
       Number of solutions $nsol$
Output: Selected Pareto front $pf\_sel$,
        Selected Pareto set $ps\_sel$
Normalize $pf$
Find the ideal point of the Pareto front $\min(norm(pf))$.
Calculate the distance $d$ from the ideal point to a point in the Pareto front
Find $d_{\max}$ and $d_{\min}$
Calculate $h = \frac{d_{\max} - d_{\min}}{nDiv}$
$r \longleftarrow d_{\min}$
while $r \leq d_{\max}$ and $n < nsol$
    Cut $pf$ with a circle of radius $r$ and its center at the ideal point
    for $d \leq r$
        $n \leftarrow n + 1$
        $pf\_sel \longleftarrow pf(d)$
        $ps\_sel \longleftarrow ps(d)$
    end for
    $r \longleftarrow r + h$
end while
Denormalize $pf\_sel$
```

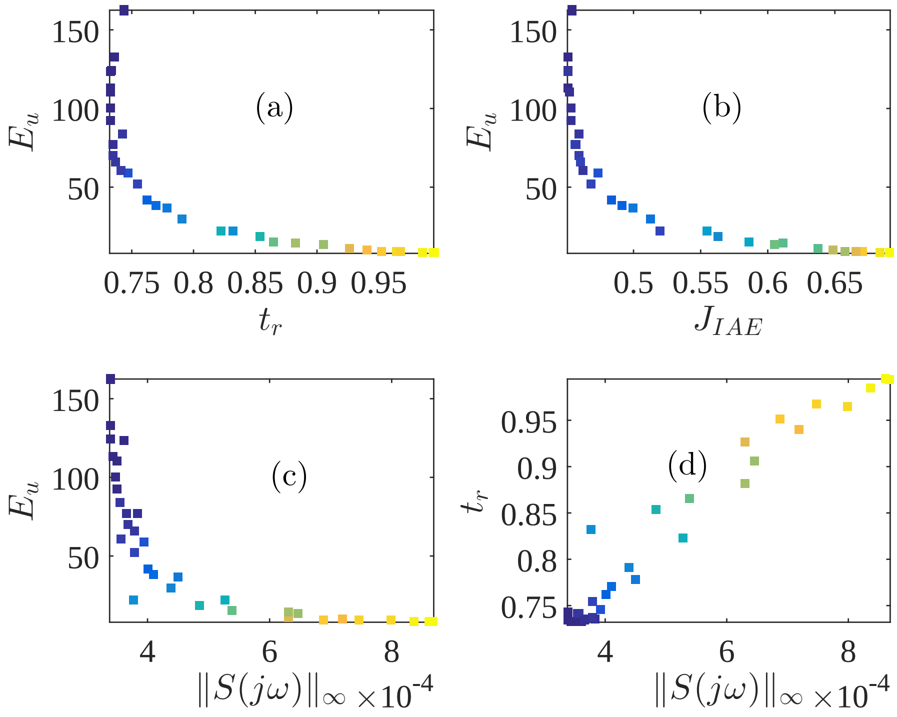

Figure 5.1: Different projections of the *Pareto front*: (a) E_u versus t_r, (b) E_u versus the J_{IAE}, (c) E_u versus $\|S(j\omega)\|_\infty$, (d) t_r versus $\|S(j\omega)\|_\infty$.

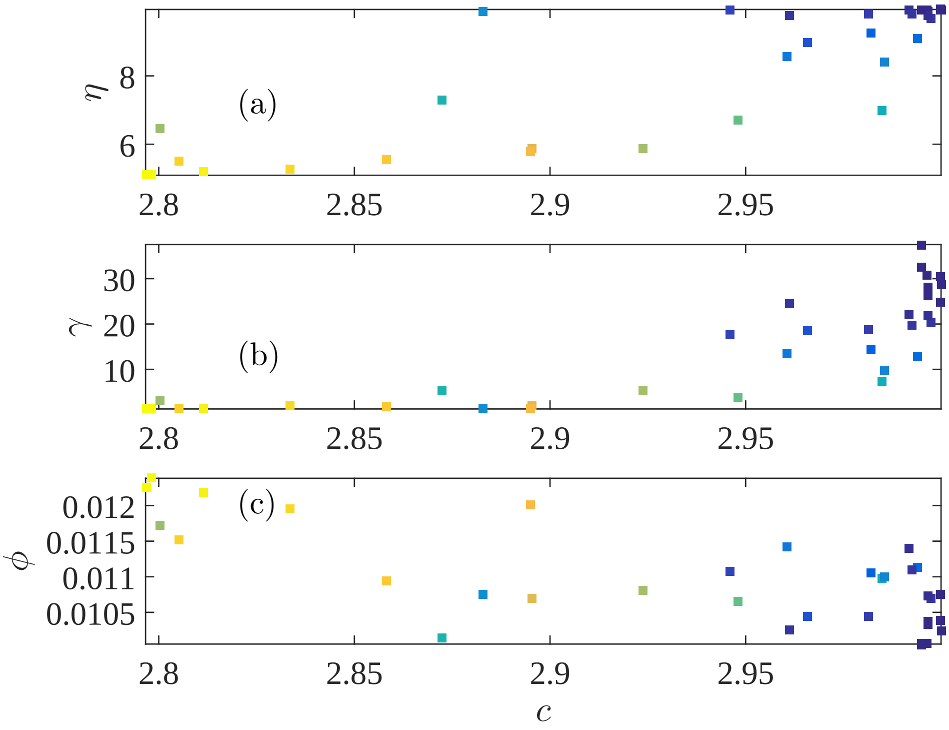

Figure 5.2: The Pareto set: (a) η versus c, (b) γ versus c, (c) ϕ versus c.

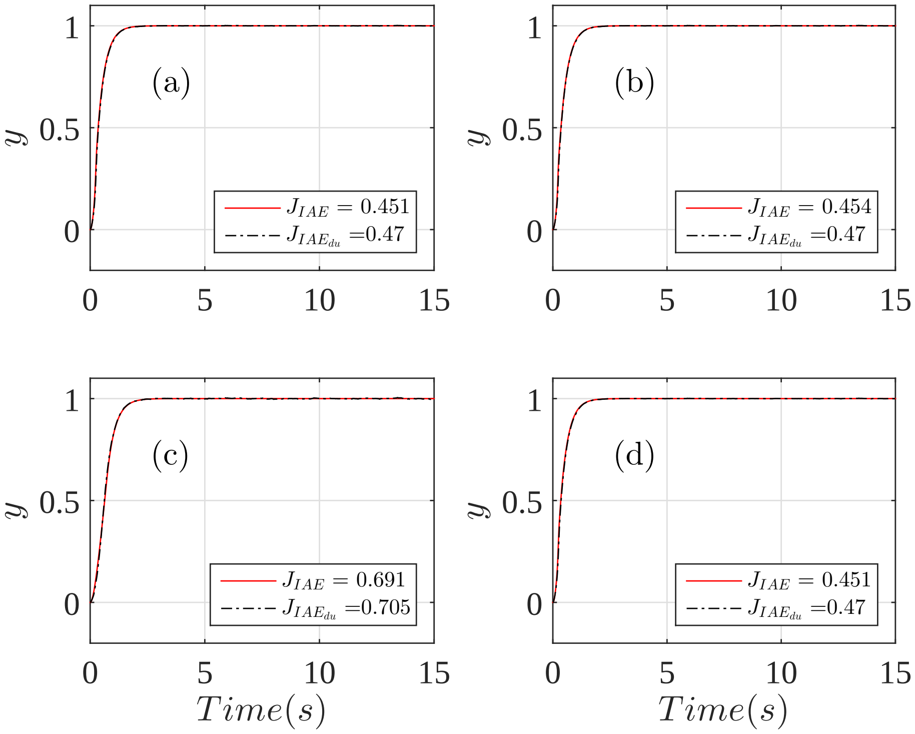

Figure 5.3: System responses before (red solid line) and after (black dashed-dotted line) adding both an external disturbance and 20% uncertainty in the model parameters under the control with (a) minimum t_r, (b) minimum $\|S(j\omega)\|_\infty$, (c) minimum E_u, (d) minimum J_{IAE}.

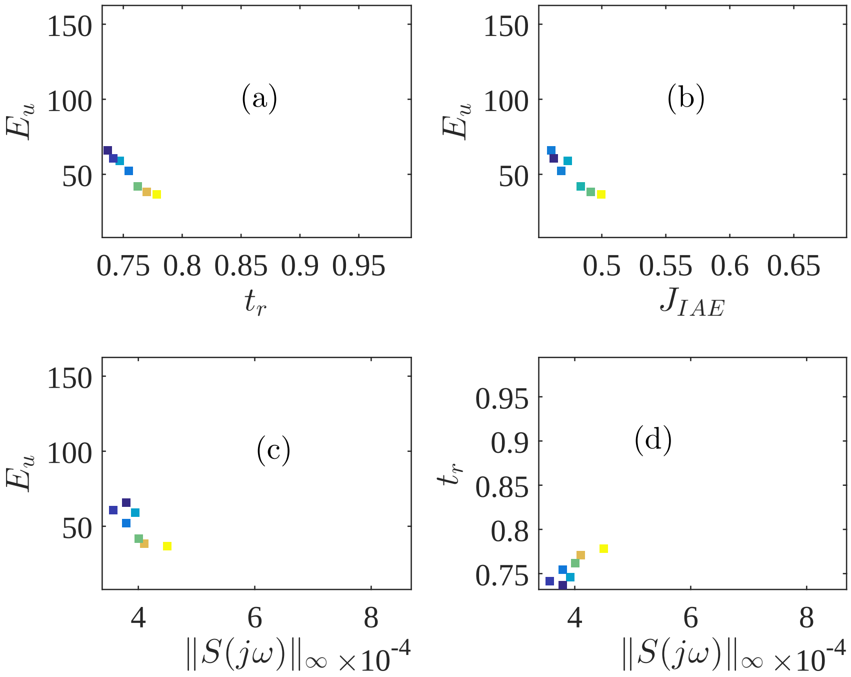

Figure 5.4: The top 20% of the Pareto front in Figure 5.1

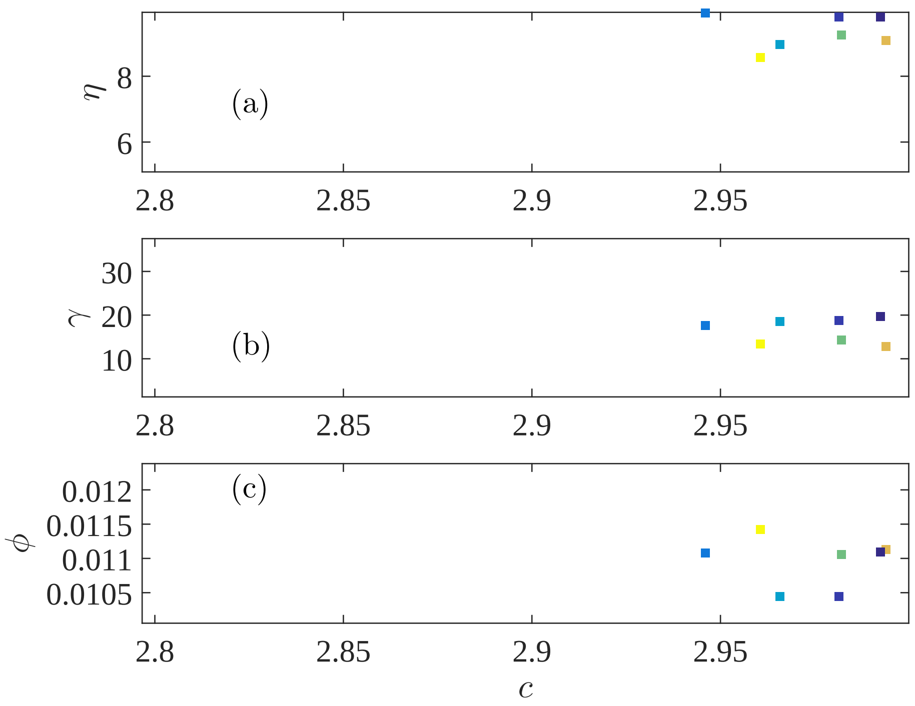

Figure 5.5: The Pareto set corresponding to the Pareto front of Figure 5.4

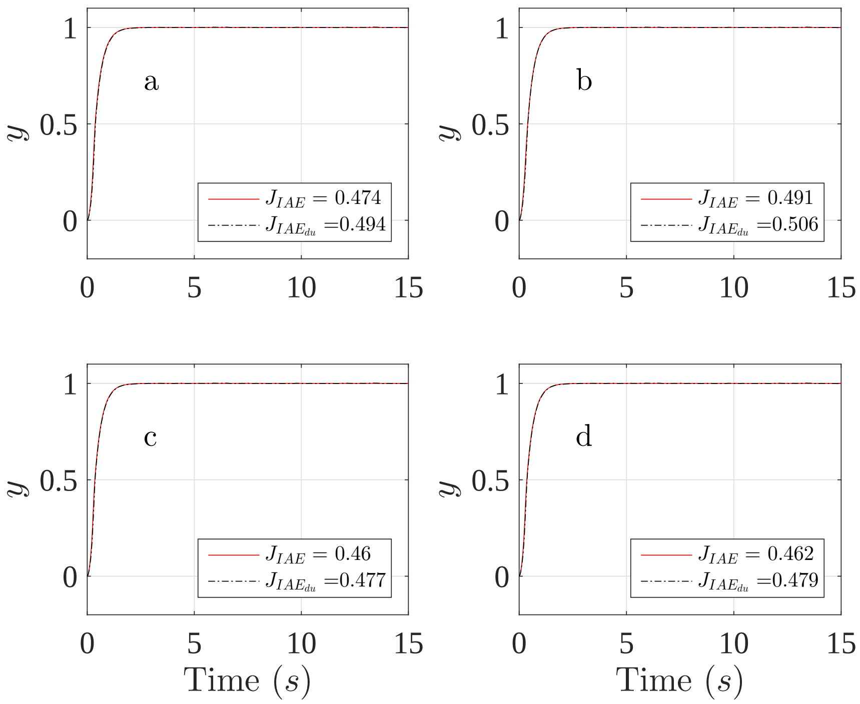

Figure 5.6: System responses before (red solid line) and after (black dashed-dotted line) adding both an external disturbance and 20% uncertainty in the model parameters under four randomly chosen controls from the Pareto set in Figure 5.5.

Chapter 6

A MULTI-OBJECTIVE OPTIMAL PID CONTROL FOR THE DUFFING SYSTEM WITH TIME DELAY

6.1 Introduction

There have been many studies of feedback controls of dynamic systems with time delay. It is particularly difficult to explicitly design feedback controls of nonlinear systems with time delay to meet time domain specifications such as rise time, overshoot and tracking error. Furthermore, these time domain specifications tend to be conflicting to each other to make the optimal feedback control design even more challenging.

In this chapter, we use the SCM method proposed in Section 2.3 for multi-objective optimal design of a delayed PID control applied to a Duffing system. Such a control problem has not been studied before to our best knowledge. In particular, we consider the time domain specifications of PID control for the Duffing system.

6.2 Time-Delayed Control System

Consider a second order nonlinear dynamic system with time delays given by,

$$\begin{aligned} \dot{x}_1 &= x_2 \\ \dot{x}_2 &= f\left(x_1, x_2, x_1\left(t-\tau_s\right), x_2\left(t-\tau_s\right)\right) + u\left(t-\tau_c\right), \end{aligned} \tag{6.1}$$

where f is a nonlinear function of its arguments. τ_s is a system delay, and τ_c is a control delay. We consider a PID feedback control given by

$$u(t) = k_p\left[r(t) - x_1(t)\right] + k_i \int_0^t \left[r(\hat{t}) - x_1(\hat{t})\right] d\hat{t} - k_d x_2(t), \tag{6.2}$$

where $r(t)$ is a reference input, k_p, k_i and k_d are the PID control gains. We introduce a third state variable x_3 such that $\dot{x}_3(t) = r(t) - x_1(t)$. The extended system is governed by the following equations.

$$\begin{aligned} \dot{x}_1 &= x_2, \\ \dot{x}_2 &= f\left(x_1, x_2, x_1\left(t-\tau_s\right), x_2\left(t-\tau_s\right)\right) + u\left(t-\tau_c\right), \\ \dot{x}_3 &= r(t) - x_1(t), \end{aligned} \tag{6.3}$$

where

$$u(t) = k_p \left[r(t) - x_1(t)\right] + k_i x_3 - k_d x_2(t). \tag{6.4}$$

Assume that the closed-loop system is stable and $r(t)$ is a step function. In steady-state, we have a unique equilibrium solution,

$$\begin{aligned} &x_1^* = 1, \quad x_2^* = 0, \\ &x_3^* = -\frac{1}{k_i} f(1, 0, 1, 0). \end{aligned} \tag{6.5}$$

It should be pointed out that the uncontrolled nonlinear system may have multiple equilibrium solutions. The stability of the steady state response can be analyzed by linearizing the system. Let $\mathbf{z} = [z_1, z_2, z_3]^T$ be the perturbation of the system away from the steady state $\mathbf{x}^* = [x_1^*, x_2^*, x_3^*]^T$. We have

$$\dot{\mathbf{z}}(t) = \mathbf{A}\mathbf{z}(t) + \mathbf{A}_s\mathbf{z}\left(t - \tau_s\right) + \mathbf{A}_c\mathbf{z}\left(t - \tau_c\right), \tag{6.6}$$

where $\mathbf{A}$, $\mathbf{A}_s$ and $\mathbf{A}_c$ are matrices of the linearized system and are functions of the control gains. The stability of the linearized system can be analyzed by the method of continuous time approximation [108, 109].

6.3 Multi-objective Optimal Design

We consider the multi-objective optimal control design with the gains $\mathbf{k} = [k_p, k_i, k_d]^T$ as design parameters for the system discussed in Section 6.2. Peak time and overshoot are common objectives in time domain control design [45, 110, 111]. We consider the MOP for the optimal control gain $\mathbf{k}$ to minimize the following three objectives

$$\min_{\mathbf{k} \in Q} \{t_p, M_p, e_{IAE}\} \text{ subject to the stability of the system (6.6)}, \tag{6.7}$$

where M_p stands for the overshoot of the response to a step reference input, t_p is the corresponding peak time and e_{IAE} is the integrated absolute tracking error

$$e_{IAE} = \int_0^{T_{ss}} \left| r(\hat{t}) - x_1(\hat{t}) \right| d\hat{t}. \tag{6.8}$$

where $r(t)$ is a reference input and T_{ss} is the time when the response is close to be in the steady state. The closed-loop response of the system for each design trial can be computed with the help of numerical integration programs of delayed differential equations.

6.4 A Numerical Example

Consider the Duffing system given by

$$f\left(x_1, x_2, x_1\left(t-\tau_s\right), x_2\left(t-\tau_s\right)\right) = -ax_1 - bx_1^3 - cx_2, \tag{6.9}$$

where $a = -1$, $b = 0.25$ and $c = 0.01$. Note that the system at the origin of the state space is unstable. The control time delay is 0.05 seconds. The system is under the delayed PID control in Equation (6.4). We study the multi-objective optimization problem defined in Equation (6.7) to design the control gain $\mathbf{k}$. The time-domain response of the Duffing system for each selection of the control gain is generated with the delayed differential equation integration algorithm (dde23) in Matlab. The integrated absolute tracking error e_{IAE} is calculated over time with $T_{ss} = 4$ seconds. The design space for the parameters is chosen as follows,

$$Q = \{\mathbf{k} \in [80, 120] \times [10, 30] \times [10, 30] \subset \mathbf{R}^3\}. \tag{6.10}$$

We impose the constraints

$$[t_p, M_p, e_{IAE}, \lambda_{ss}] \leq [2.5, 6\%, 0.75, -0.25], \tag{6.11}$$

where λ_{ss} denotes the largest real part of the eigenvalues of the linearized steady-state system (6.6). The eigenvalues of the linearized system are computed with the method of continuous time approximation and the Chebyshev interpolation [108, 112]. The constraint on the eigenvalues is intended to provide the stability robustness of the optimized control system. Since the original system is nonlinear, the stability condition should be imposed on the steady-state equilibrium solutions.

Initially, we select the number of divisions of the three control gain space as $\mathbf{N} = [30, 15, 15]$. The cells of the rough Pareto set is sub-divided into 27 cells ($3 \times 3 \times 3$). The first run of the SCM method on the rough grid finds 460 cells representing the Pareto set shown in Figure 6.1. The corresponding Pareto front is shown in Figure 6.2. The CPU time of the first run is 1382.4 seconds. The second run on the sub-divided cells finds the Pareto set with 2386 cells shown in Figure 6.3. The refined Pareto front is shown in Figure 6.4. The CPU time of the second run is 5695.5 seconds.

We should point out that the Pareto fronts obtained by the SCM method have fine global structures. Such fine structures of Pareto fronts are not often found in the literature before. Finally, we present an example of step response under the delayed control with the gain $[k_p, k_i, k_d] = [82.4444, 21.7778, 14.2222]$. The result is shown in Figure 6.5. The step response shows excellent time-domain performance with $[t_p, M_p, e_{IAE}, \lambda_{ss}] = [0.3300, 4.8829\%, 0.2155, -0.2781]$.

6.5 Concluding Remarks

We have presented a multi-objective PID control design for the Duffing system by using the simple cell mapping (SCM) method applied to MOPs. The time-domain specifications of the step response are used as the objective functions. A constraint on the closed-loop eigenvalue of the linearized system about the steady-state equilibrium solution is also imposed that provides the stability robustness of the optimized PID controls. The SCM method is implemented in a hybrid manner as described earlier. In the first run of the hybrid algorithm, the SCM method delivers a set of cells that cover the Pareto set. In the second run, a gradient search is applied to the covering set of cells and delivers much fine resolution of the global optimal solutions of Pareto set and Pareto front. We have found that the hybrid algorithm for the SCM method delivers substantial computational savings while obtaining comparably accurate solutions for the Pareto set and Pareto front.

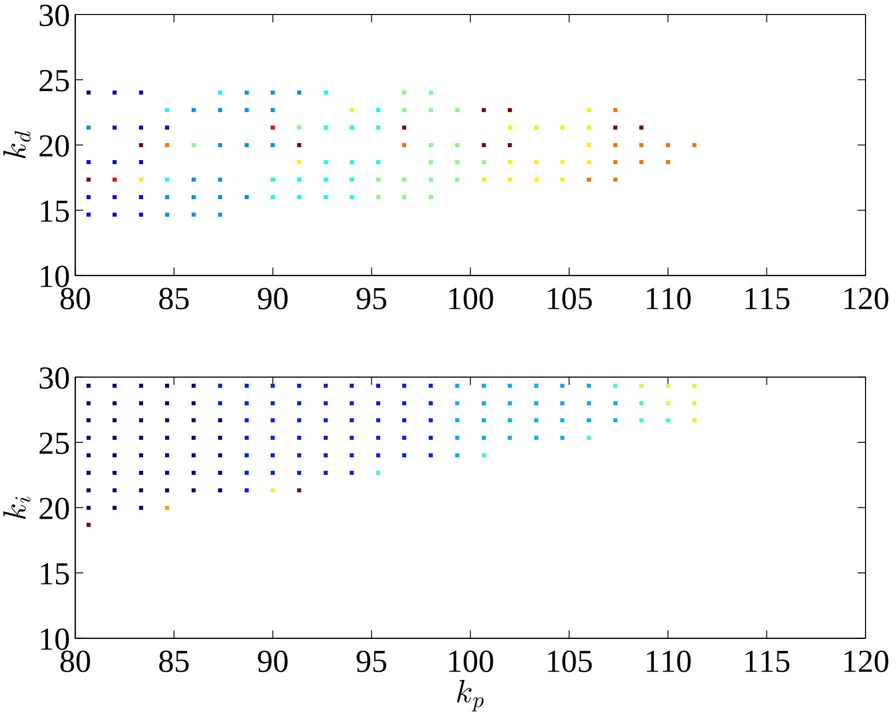

Figure 6.1: The Pareto set obtained on the rough grid by the SCM method for the Duffing system with delayed control.

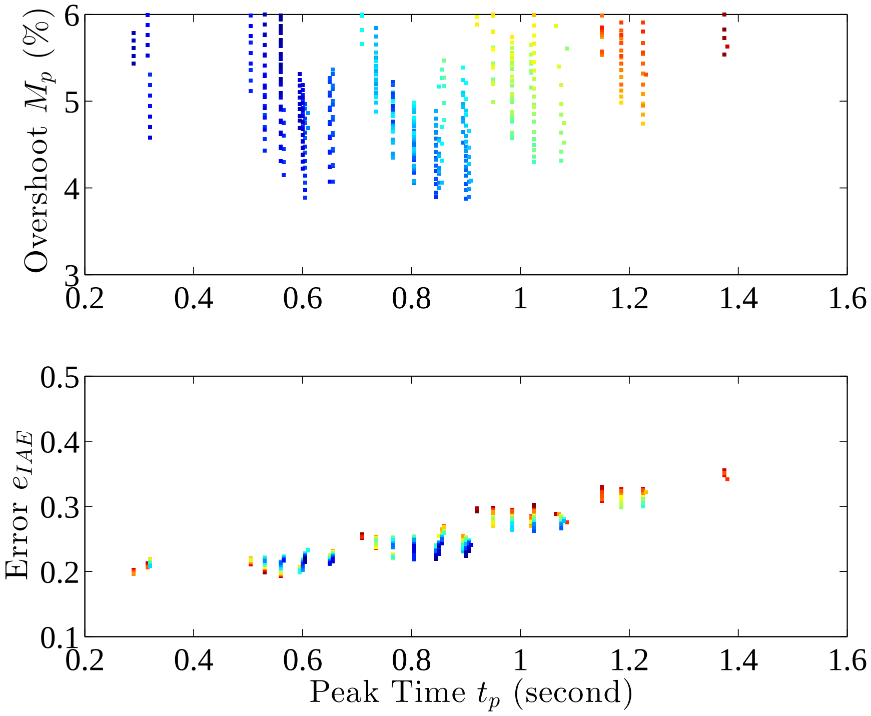

Figure 6.2: The Pareto front of the Duffing system corresponding to the Pareto set in Figure 6.1.

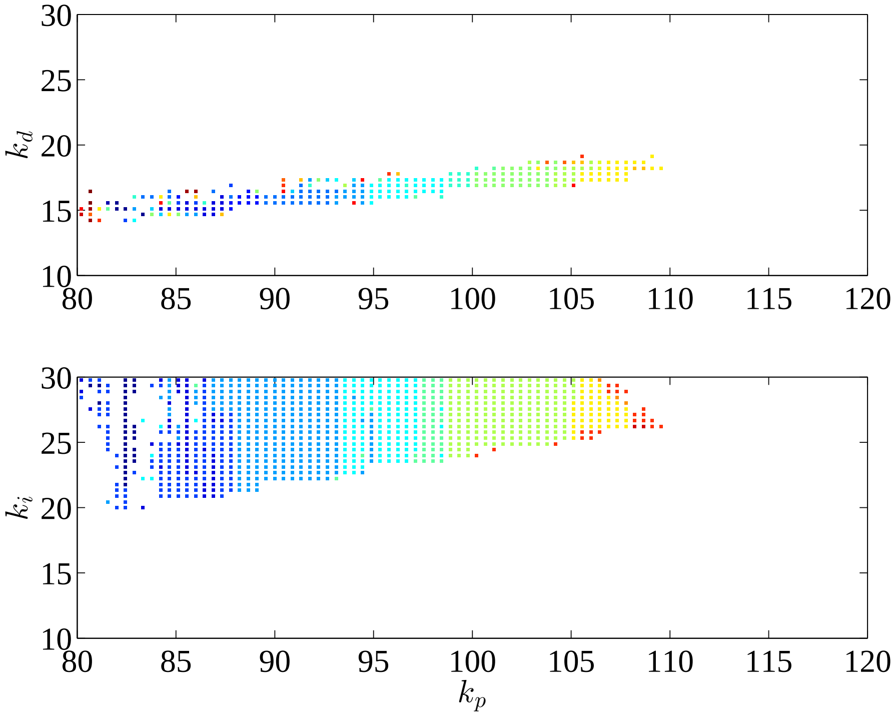

Figure 6.3: The refined Pareto set shown in Figure 6.1 of the Duffing system with delayed control by the SCM method.

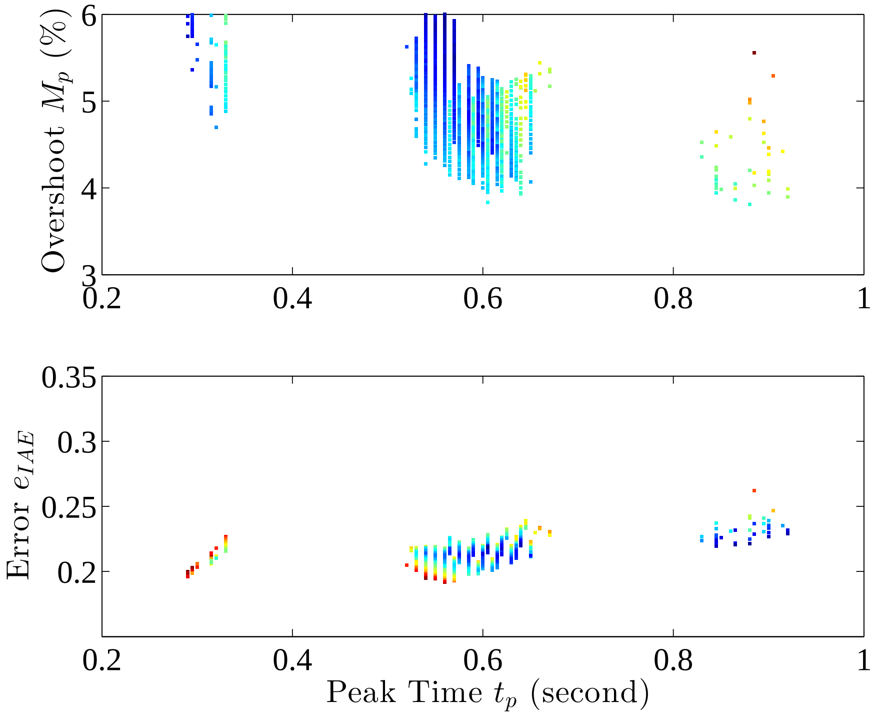

Figure 6.4: The refined Pareto front of the Duffing system corresponding to the Pareto set in Figure 6.3.

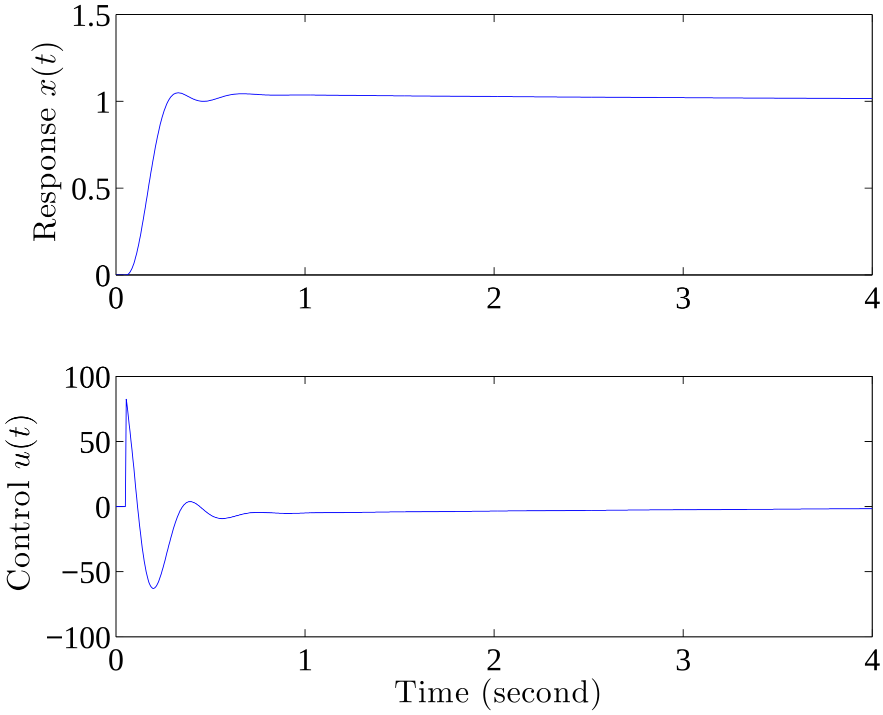

Figure 6.5: An example of the step response of the Duffing system under the delayed PID control with $[k_p, k_i, k_d] = [82.4444, 21.7778, 14.2222]$.

Chapter 7

FUTURE WORK

My future research would expand to include the use of the multi-objective optimization concept in the design of real-life applications including, but not limited to, robotics, cruise control systems, and aircrafts. The optimization of these systems involves many conflicting objectives. In robotics, designing a robot that has the highest possible speed of response, smallest tracking error and lowest energy expenditure is a challenging mission. In cruise control system design, objectives such as small tracking error, low fuel consumption and high ride comfort are well-known conflicting goals. In aircrafts, the aerodynamic design of airfoils and wings involve competing design objectives such as maximization of lift to drag ratio and rate of change of lift to attack angle to increase the lift at takeoff/landing condition and minimization of pitching moment.

I also plan to explore the area of multi-objective optimization of high dimensional problems such as the fuzzy control systems. Such systems incorporate a large number of design parameters, which means a huge computational effort is needed to tune them.

Another interesting field is the multi-objective optimal design of fractional-order controls. These controllers introduce more free parameters to be tuned compared to their counterparts of integer order control systems.

Both of the SCM method and the hybrid algorithm of the NSGA-II and SCM can be used to solve these problems accurately regardless of their complexity, and guarantee the discovery of the global Pareto optimal solutions.

Appendix A

MATRICES OF THE BOGIE SYSTEM

The matrices of the bogie system in Equation (4.1) are listed below.

$$\mathbf{M} = \begin{bmatrix} m_w &&&&&&& \\ & I_w &&&&&& \\ && m_w &&&&& \\ &&& I_w &&&& \\ &&&& m_f &&& \\ &&&&& I_f && \\ &&&&&& m_d & \\ &&&&&&& m_d \end{bmatrix}$$

$$\mathbf{C} = \begin{bmatrix} \frac{2f\eta}{v} &&&&&&& \\ & \frac{2l_0^2 f_\zeta}{v} &&&&&& \\ && \frac{2f\eta}{v} &&&&& \\ &&& \frac{2L_0^2 f_\zeta}{v} &&&& \\ &&&& c_{sy} + 2c_y && -c_y & -c_y \\ &&&&& l_2^2 c_{sx} + l_m^2 c_y & -l_m c_y & l_m c_y \\ &&&& -c_y & -l_m c_y & c_y & \\ &&&& -c_y & l_m c_y && c_y \end{bmatrix}$$

$$\mathbf{E} = \begin{bmatrix} 0 & 0 & 0 & 0 & 1 & l_e & 0 & 0 \\ 0 & 0 & 0 & 0 & 1 & -l_e & 0 & 0 \end{bmatrix}^T$$

$$\mathbf{K} = \begin{bmatrix} k_{py}+k_{gy} & -2f\eta & & & -k_{py} & -bk_{py} & & \\ \frac{2\lambda_e l_0 f_\zeta}{r_0} & l_1^2 k_{px}+k_{g\psi} & & & & -l_1^2 k_{px} & & \\ & & k_{py}+k_{gy} & -2f\eta & -k_{py} & bk_{py} & & \\ & & \frac{2\lambda_e l_0 f_\zeta}{r_0} & l_1^2 k_{px}+k_{g\psi} & & -l_1^2 k_{px} & & \\ -k_{py} & & -k_{py} & & 2k_{py}+k_{sy}+2k_y & & -k_y & -k_y \\ -bk_{py} & -l_1^2 k_{px} & bk_{py} & -l_1^2 k_{px} & & l_2^2 k_{sx}+2l_1^2 k_{px}+2b^2 k_{py}+2l_m^2 k_y & -l_m k_y & l_m k_y \\ & & & & -k_y & -l_m k_y & k_y & \\ & & & & -k_y & l_m k_y & & k_y \end{bmatrix}$$

Table A.1: The bogie model parameters.

Symbol	Definition	Value
m_w	Mass of the wheelset	285 kg
I_w	Yaw inertia of the wheelset yaw inertia	2024 $kg.m^2$
m_f	Mass of bogie & non-flexible part of the drive system	7186 kg
I_f	Yaw inertia of bogie & non-flexible part of the drive system	9571 $kg.m^2$
m_d	Mass of flexible suspended part of the drive system	1765 kg
I_d	Yaw inertia of flexible suspended part of the drive system	1019 $kg.m^2$
l_e	Distance between the actuator and bogie center	1.5 m
l_m	the longitudinal distance from motor to bogie center	0.5 m
k_{px}	Primary longitudinal stiffness per axle	40 kN/mm
k_{py}	Primary lateral stiffness per axle	6 kN/mm
k_{sx}	Secondary longitudinal stiffness	0.8 kN/mm
k_{sy}	Secondary lateral stiffness	0.8 kN/mm
c_{sx}	Secondary longitudinal damping	1000 $N.s/m$
c_{sy}	Secondary lateral damping	60 $kN.s/m$
$2b$	Wheel base	2.5 m
$2l_0$	Distance of the Contact spot	1493 mm
$2l_1$	Lateral spacing of the primary suspension	2200 mm
$2l_2$	Lateral spacing of the secondary suspension	2200 mm
r_0	The wheel rolling radius	0.625 m
λ_e	The wheel-rail contact conicity	0.15
f_ζ	The longitudinal creep coefficient	8.624e6 N
f_η	The lateral creep coefficient	8.144e6 N
k_{gy}	The gravitational stiffness	41.4 kN/m
$k_{g\psi}$	The gravitational angular stiffness	-23 kN/rad
k_r	The contact stiffness of the wheel-rail	50 kN/mm

BIBLIOGRAPHY

[1] V. Pareto, Manual of Political Economy, The MacMillan Press, London, 1971 (original edition in French in 1927).

[2] D. F. Jones, S. K. Mirrazavi, M. Tamiz, Multi-objective meta-heuristics: An overview of the current state-of-the-art, European Journal of Operational Research 137 (1) (2002) 1–9.

[3] R. T. Marler, J. S. Arora, Survey of multi-objective optimization methods for engineering, Structural and multidisciplinary optimization 26 (6) (2004) 369–395.

[4] J. L. Cohon, Multicriteria programming: Brief review and application, Design optimization Edited by J.S. Gero, Academic Press, Inc. (1985) 163–191.

[5] R. E. Rosenthal, Principles of Multiobjective Optimization, Decision Sciences 16 (2) (1985) 133–152.

[6] D. G. Carmichael, Structural modelling and optimization: a general methodology for engineering and control, Ellis Horwood, 1981.

[7] K. Miettinen, Nonlinear multiobjective optimization, Springer Science & Business Media, 2012.

[8] A. Gambier, M. Jipp, Multi-objective optimal control: An introduction, in: Proceedings of the 8th Asian Control Conference, 2011, pp. 1084–1089.

[9] A. Gambier, MPC and PID control based on multi-objective optimization, in: Proceedings of American Control Conference, 2008, pp. 4727–4732.

[10] S. Gass, T. Saaty, The computational algorithm for the parametric objective function, Naval research logistics quarterly 2 (1-2) (1955) 39–45.

[11] L. Zadeh, Optimality and non-scalar-valued performance criteria, IEEE Transactions on Automatic Control 8 (1) (1963) 59–60.

[12] F. Gembicki, Y. Haimes, Approach to performance and sensitivity multiobjective optimization: The goal attainment method, IEEE Transactions on Automatic Control 20 (6) (1975) 769–771.

[13] A. Ben-Tal, Characterization of Pareto and lexicographic optimal solutions, Springer, 1980.

[14] G. P. Liu, J.-B. Yang, J. F. Whidborne, Multiobjective optimisation and control .

[15] C. A. Coello Coello, G. Lamont, D. A. Van Veldhuizen, Evolutionary Algorithms for Solving Multi-Objective Problems, Springer, New York, 2007.

[16] C. Hernández, Y. Naranjani, Y. Sardahi, W. Liang, O. Schütze, J.-Q. Sun, Simple cell mapping method for multi-objective optimal feedback control design, International Journal of Dynamics and Control 1 (3) (2013) 231–238.

[17] D. E. Goldberg, J. H. Holland, Genetic algorithms and machine learning, Machine learning 3 (2) (1988) 95–99.

[18] G. Reinelt, The traveling salesman: computational solutions for TSP applications, Springer-Verlag, 1994.

[19] C. M. M. d. Fonseca, Multiobjective genetic algorithms with application to control engineering problems, Ph.D. thesis, University of Sheffield (1995).

[20] J. Moore, R. Chapman, Application of particle swarm to multiobjective optimization, Department of Computer Science and Software Engineering, Auburn University 32.

[21] K. Deb, S. Agrawal, A. Pratap, T. Meyarivan, A fast elitist non-dominated sorting genetic algorithm for multi-objective optimization: NSGA-II, in: Proceedings of Parallel Problem Solving from Nature PPSN VI, 2000, pp. 849–858.

[22] Z. E., M. Laumanns, L. Thiele, Spea2: Improving the strength pareto evolutionary algorithm, Tech. Rep. 103 (2001).

[23] M. Erickson, A. Mayer, J. Horn, The niched pareto genetic algorithm 2 applied to the design of groundwater remediation systems, in: Proceedings of Evolutionary Multi-Criterion Optimization, 2001, pp. 681–695.

[24] O. Schütze, M. Vasile, O. Junge, M. Dellnitz, D. Izzo, Designing optimal low thrust gravity assist trajectories using space pruning and a multi-objective approach, Engineering Optimization 41 (2) (2009) 155–181.

[25] C. S. Hsu, Cell-to-Cell Mapping, A Method of Global Analysis for Nonlinear Systems, Springer-Verlag, New York, 1987.

[26] L. V. Santana-Quintero, A. G. Hernández-Diáz, J. a. Molina, C. A. C. Coello, R. Caballero, Demors: A hybrid multi-objective optimization algorithm using differential evolution and rough set theory for constrained problems, Computers & Operations Research 37 (3) (2010) 470–480.

[27] V. Barichard, J.-K. Hao, Un algorithme hybride pour le probéme de sac á dos multi-objectifs, Huitiemes Journées Nationales sur la Résolution Pratique de Problemes NP-Complets JNPC .

[28] P. Engrand, A multi-objective optimization approach based on simulated annealing and its application to nuclear fuel management, Tech. rep., Electricite de France (1998).

[29] P. Czyzżak, A. Jaszkiewicz, Pareto simulated annealing-A metaheuristic technique for multiple-objective combinatorial optimization, Journal of Multi-Criteria Decision Analysis 7 (1) (1998) 34–47.

[30] M. Ehrgott, X. Gandibleux, Hybrid metaheuristics for multi-objective combinatorial optimization, in: Hybrid metaheuristics, Springer, 2008, pp. 221–259.

[31] Y. Y. Haimes, L. S. Ladson, D. A. Wismer, Bicriterion formulation of problems of integrated system identification and system optimization, IEEE Transactions on Systems Man and Cybernetics (1) (1971) 296–297.

[32] J. D. Schaffer, Multiple objective optimization with vector evaluated genetic algorithms, in: Proceedings of the 1st international Conference on Genetic Algorithms, 1985, pp. 93–100.

[33] C. M. Fonseca, P. J. Fleming, Genetic algorithms for multiobjective optimization: Formulation, discussion and generalization, in: Proceedings of ICGA, Vol. 93, 1993, pp. 416–423.

[34] A. Gambier, E. Badreddin, Multi-objective optimal control: An overview, in: Proceedings of the 16th IEEE International Conference on Control Applications, Singapore, 2007, pp. 170–175.

[35] A. Popov, A. Farag, H. Werner, Tuning of a PID controller using a multi-objective optimization technique applied to a neutralization plant, in: Proceedings of IEEE Conference on Decision and Control and the 44th European Control Conference, 2005, pp. 7139–7143.

[36] M. Rani, H. Selamat, H. Zamzuri, Z. Ibrahim, Multi-objective optimization for PID controller tuning using the global ranking genetic algorithm, International Journal of Innovative computing, Information and Control 8 (1) (2012) 269–284.

[37] M. Khoie, A. Sedigh, K. Salahshoor, PID controller tuning using multi-objective optimization based on fused genetic-immune algorithm and immune feedback mechanism, International Conference on Mechatronics and Automation (2011) 2459–2464.

[38] C. A. Kumar, N. K. Nair, NSGA-II based multiobjective PID controller tuning for speed control of DC motor drives, International Journal of Soft Computing 5 (3) (2010) 83–87.

[39] C. Ibtissem, L. Noureddine, B. Pierre, Tuning PID controller using multiobjective ant colony optimization, Applied Computational Intelligence and Soft Computing 10.1155/2012/536326.

[40] D. H. Kim, Tuning of PID controller using gain/phase margin and immune algorithm, in: Proceedings of the 2005 IEEE Mid-Summer Workshop on Soft Computing in Industrial Applications, 2005, pp. 69–74.

[41] A.-G. Esmaeil, L. Caro, Designing an optimal PID controller using imperialist competitive algorithm, Intelligent Systems Scientific Society of Iran 1 (2007) 1–6.

[42] G. K. M. Pedersen, Z. Yang, Multi-objective PID-controller tuning for a magnetic levitation system using NSGA-II, in: Proceedings of the 8th Annual Conference on Genetic and Evolutionary computation, 2006, pp. 1737–1744.

[43] N. B. C. Hutauruk, M. Brown, Directed multi-objective optimization for controller design, in: Proceedings of International Conference on Instrumentation, Communication and Information Technology, 2005, pp. 3–5.

[44] G. P. Liu, J. F. Whidborne, G. R. Duan, Multiobjective design using various control techniques, in: Proceedings of IEEE International Symposium on Computer Aided Control System Design, 2002, pp. 1–6.

[45] G. P. Liu, S. Daley, Optimal-tuning PID controller design in the frequency domain with application to a rotary hydraulic system, Control Engineering Practice 7 (7) (1999) 821–830.

[46] L. K. Kookos, A. I. Lygeros, K. G. Arvanitis, PI controller tuning via multiobjective optimisation, Journal A 40 (2) (1999) 30–36.

[47] J. S. Baras, M. K. H. Fan, W. T. Nye, A. L. Tits, DELIGHT LQG: A CAD system for control system design using LQG controller structure, in: Proceedings of the 18th Annual Conference on Information Science and Systems, 1984.

[48] D. Haessig, Selection of LQG/LTR weighting matrices through constrained optimization, in: Proceedings of the American Control Conference, Vol. 1, 1995, pp. 458–460.

[49] G. P. Liu, R. J. Patton, Robust control design using eigenstructure assignment and multi-objective optimization, International Journal of Systems Science 27 (9) (1996) 871–879.

[50] J. Dai, J. Ying, C. Tan, A novel particle swarm optimization based robust H-infinity control for rotorcrafts, Engineering Computations 31 (4) (2014) 726–741.

[51] M. Alitavoli, M. Taherkhorsandi, M. J. Mahmoodabadi, A. Bagheri, B. Miripour-Fard, Pareto design of sliding-mode tracking control of a biped robot with aid of an innovative particle swarm optimization, in: Proceedings of International Symposium on Innovations in Intelligent Systems and Applications, 2012, pp. 1–5.

[52] M. Sharifi, a. Rezapur, B. Shahriari, Optimization of sliding mode control for a vehicle suspension system via multi-objective genetic algorithm with uncertainty, Journal of Basic and Applied Scientific Research 2 (7) (2012) 6724–6729.

[53] Y. Li, K. C. Ng, D. J. Murray-Smith, G. J. Gray, K. C. Sharman, Genetic algorithm automated approach to the design of sliding mode control systems, International Journal of Control 63 (4) (1996) 721–739.

[54] A. Trebi-Ollennu, B. A. White, Multiobjective fuzzy genetic algorithm optimisation approach to nonlinear control system design, IEE Proceedings - Control Theory and Applications 144 (2) (1997) 137–142.

[55] M. A. Costa, A. P. Braga, B. R. Menezes, R. A. Teixeira, G. G. Parma, Training neural networks with a multi-objective sliding mode control algorithm, Neurocomputing 51 (2003) 467–473.

[56] H.-S. Kim, P. N. Roschke, Fuzzy control of base-isolation system using multi-objective genetic algorithm, Computer-Aided Civil and Infrastructure Engineering 21 (6) (2006) 436–449.

[57] J. H. Crews, M. G. Mattson, G. D. Buckner, Multi-objective control optimization for semi-active vehicle suspensions, Journal of Sound and Vibration 330 (23) (2011) 5502–5516.

[58] M. J. Mahmoodabadi, S. A. Mostaghim, A. Bagheri, N. Nariman-zadeh, Pareto optimal design of the decoupled sliding mode controller for an inverted pendulum system and its stability simulation via java programming, Mathematical and Computer Modelling 57 (56) (2013) 1070–1082.

[59] S. Mostaghim, J. Teich, Strategies for finding good local guides in multi-objective particle swarm optimization (MOPSO), IEEE Proceedings Symposium on Swarm Intelligence (2003) 26–33.

[60] K. Atashkari, N. Nariman-Zadeh, M. Gölcü, A. Khalkhali, A. Jamali, Modelling and multi-objective optimization of a variable valve-timing spark-ignition engine using polynomial neural networks and evolutionary algorithms, Energy Conversion and Management 48 (3) (2007) 1029–1041.

[61] M. J. Mahmoodabadi, M. Taherkhorsandi, A. Bagheri, Optimal robust sliding mode tracking control of a biped robot based on ingenious multi-objective pso, Neurocomputing 124 (2014) 194–209.

[62] Z.-C. Qin, F.-R. Xiong, Q. Ding, C. Hernández, J. u. Fernandez, O. Schütze, J.-Q. Sun, Multi-objective optimal design of sliding mode control with parallel simple cell mapping method, Journal of Vibration and Control (2015) 1077546315574948.

[63] F. Y. Cheng, D. Li, Multiobjective optimization design with pareto genetic algorithm, Journal of Structural Engineering 123 (9) (1997) 1252–1261.

[64] S. Rao, V. B. Venkayya, N. S. Khot, Game theory approach for the integrated design of structures and controls, AIAA Journal 26 (4) (1988) 463–469.

[65] A. Messac, B. Wilsont, Physical programming for computational control, AIAA Journal 36 (2) (1998) 219–226.

[66] N. Srinivas, K. Deb, Multiobjective optimization using nondominated sorting in genetic algorithms, Evolutionary Computation 2 (3) (1994) 221–248.

[67] K. Deb, A. Pratap, S. Agarwal, T. Meyarivan, A fast and elitist multiobjective genetic algorithm: NSGA-II, IEEE Transactions on Evolutionary Computation 6 (2) (2002) 182–197.

[68] H. G. Beyer, K. Deb, On self-adaptive features in real-parameter evolutionary algorithms, IEEE Transactions on Evolutionary Computation 5 (3) (2001) 250–270.

[69] K. Deb, R. B. Agrawal, Simulated binary crossover for continuous search space, Complex Systems 9 (2) (1995) 115–148.

[70] M. M. Raghuwanshi, O. G. Kakde, Survey on multiobjective evolutionary and real coded genetic algorithms, in: Proceedings of the 8th Asia Pacific Symposium on Intelligent and Evolutionary Systems, 2004, pp. 150–161.

[71] R. L. Haupt, S. E. Haupt, Practical genetic algorithms, John Wiley & Sons, 2004.

[72] O. Schütze, A. Lara, C. A. C. Coello, The directed search method for unconstrained multi-objective optimization problems, Ph.D. thesis (2011).

[73] A. Lara, S. Alvarado, S. Salomon, G. Avigad, C. A. C. Coello, O. Schütze, The gradient free directed search method as local search within multi-objective evolutionary algorithms, EVOLVE - A Bridge between Probability, Set Oriented Numerics, and Evolutionary Computation (EVOLVE II) (2013) 153–168.

[74] I. Das, J. Dennis, *Normal-boundary intersection*: A new method for generating the Pareto surface in nonlinear multicriteria optimization problems, SIAM Journal of Optimization 8 (1998) 631–657.

[75] J. Nocedal, S. Wright, Numerical Optimization, Springer, 2006.

[76] C. S. Hsu, A discrete method of optimal control based upon the cell state space concept, Journal of Optimization Theory and Applications 46 (4) (1985) 547–569.

[77] F. H. Bursal, C. S. Hsu, Application of a cell-mapping method to optimal control problems, International Journal of Control 49 (5) (1989) 1505–1522.

[78] F. Y. Wang, P. J. A. Lever, A cell mapping method for general optimum trajectory planning of multiple robotic arms, Robotics and Autonomous Systems 12 (1994) 15–27.

[79] R. C. Dorf, R. H. Bishop, Modern Control Systems, Prentice Hall, 2011.

[80] C. P. Ward, P. F. Weston, E. J. C. Stewart, H. Li, R. M. Goodall, C. Roberts, T. X. Mei, G. Charles, R. Dixon, Condition monitoring opportunities using vehicle-based sensors, Proceedings of the Institution of Mechanical Engineers, Part F: Journal of Rail and Rapid Transit 225 (2) (2011) 202–218.

[81] R. M. Goodall, W. Kortüm, Mechatronic developments for railway vehicles of the future, Control Engineering Practice 10 (8) (2002) 887–898.

[82] J. T. Pearson, R. M. Goodall, T. X. Mei, G. Himmelstein, Active stability control strategies for a high speed bogie, Control Engineering Practice 12 (11) (2004) 1381–1391.

[83] K. H. A. Abood, R. A. Khan, Investigation to improve hunting stability of railway carriage using semi-active longitudinal primary stiffness suspension, Journal of Mechanical Engineering Research 2 (5) (2010) 97–105.

[84] J. T. Pearson, R. M. Goodall, T. X. Mei, S. Shen, C. Kossmann, O. Polach, G. Himmelstein, Design and experimental implementation of an active stability system for a high speed bogie, Vehicle System Dynamics 41 (2004) 43–52.

[85] M. Gretzschel, A. Jaschinski, Design of an active wheelset on a scaled roller rig, Vehicle System Dynamics 41 (5) (2004) 365–381.

[86] A. H. Wickens, Comparative stability of bogie vehicles with passive and active guidance as influenced by friction and traction, Vehicle System Dynamics 47 (9) (2009) 1137–1146.

[87] T. X. Mei, R. M. Goodall, Recent development in active steering of railway vehicles, Vehicle System Dynamics 39 (6) (2003) 415–436.

[88] J. Perez, J. M. Busturia, R. M. Goodall, Control strategies for active steering of bogie-based railway vehicles, Control Engineering Practice 10 (9) (2002) 1005–1012.

[89] S. Bruni, R. Goodall, T. X. Mei, H. Tsunashima, Control and monitoring for railway vehicle dynamics, Vehicle System Dynamics 45 (7-8) (2007) 743–779.

[90] A. Alonso, J. G. Giménez, E. Gomez, Yaw damper modelling and its influence on railway dynamic stability, Vehicle System Dynamics 49 (9) (2011) 1367–1387.

[91] Y. Yao, X. Zhang, X. Liu, The active control of the lateral movement of a motor suspended under a high-speed locomotive, Proceedings of the Institution of Mechanical Engineers, Part F: Journal of Rail and Rapid Transit (2015) 0954409715605138.

[92] J. Y. Hung, W. Gao, J. C. Hung, Variable structure control: A survey, IEEE Transactions on Industrial Electronics 40 (1) (1993) 2–22.

[93] R. Cristi, F. A. Papoulias, A. J. Healey, Adaptive sliding mode control of autonomous underwater vehicles in the dive plane, IEEE Journal of Oceanic Engineering 15 (3) (1990) 152–160.

[94] Y.-J. Huang, T.-C. Kuo, S.-H. Chang, Adaptive sliding-mode control for nonlinear systems with uncertain parameters, IEEE Transactions on Systems, Man, and Cybernetics, Part B: Cybernetics 38 (2) (2008) 534–539.

[95] L. Xu, B. Yao, Adaptive robust control of mechanical systems with non-linear dynamic friction compensation, International Journal of Control 81 (2) (2008) 167–176.

[96] H. Babaee, A. Khosravi, Multi-objective COA for design robust iterative learning control via second-order sliding mode, International Journal of Control Science and Engineering 2 (6) (2012) 143–149.

[97] C. Ahn, H. Kim, Y. Kim, Adaptive sliding mode control for non-affine nonlinear vehicle systems, in: Proceedings of AIAA Guidance, Navigation and Control Conference and Exhibit, Hilton Head, South Carolina, 2007.

[98] C.-I. Ahn, Y. Kim, H. Kim, Adaptive sliding mode controller design for fault tolerant flight control system, in: Proceedings of AIAA Guidance, Navigation, and Control Conference and Exhibit, 2006.

[99] D. Zhou, C. Mu, W. Xu, Adaptive sliding-mode guidance of a homing missile, Journal of Guidance, Control, and Dynamics 22 (4) (1999) 589–594.

[100] L. Keum, N. Pradeep, S. Sahjendra, Integrated adaptive sliding mode flight control via SDU gain matrix decomposition, in: Proceedings of the 46th AIAA Aerospace Sciences Meeting and Exhibit, 2008.

[101] Q. Hu, Adaptive integral sliding mode fault tolerant control for flexible spacecraft, in: Proceedings of AIAA Guidance, Navigation, and Control Conference, Chicago, Illinois, 2009.

[102] R. M. DeSantis, An adaptive PI/sliding mode controller for a speed drive, Journal of Dynamic Systems, Measurement, and Control 111 (3) (1989) 409–415.

[103] B. Yao, M. Tomizuka, Smooth robust adaptive sliding mode control of manipulators with guaranteed transient performance, Journal of Dynamic Systems, Measurement, and Control 118 (4) (1996) 764–775.

[104] Q. Chen, L. Tao, Y. Nan, X. Ren, Adaptive nonlinear sliding mode control of mechanical servo system with LuGre friction compensation, Journal of Dynamic Systems, Measurement, and Control 138 (2) (2016) 021003.

[105] T. Ashish, Modern Control Design with Matlab and Simulink, John Wiley & Sons, 2002.

[106] M. A. Sahnehsaraei, M. J. Mahmoodabadi, M. Taherkhorsandi, Optimal robust decoupled sliding mode control based on a multi-objective genetic algorithm, in: Proceedings of IEEE International Symposium on Innovations in Intelligent Systems and Applications (INISTA), 2013, pp. 1–5.

[107] J.-J. E. Slotine, W. Li, Applied Nonlinear Control, Prentice-Hall Englewood Cliffs, New Jersey, 1991.

[108] J. Q. Sun, A method of continuous time approximation of delayed dynamical systems, Communications in Nonlinear Science and Numerical Simulation 14 (4) (2008) 998–1007.

[109] J. Q. Sun, B. Song, Some control studies of dynamical systems with time delay, in: A. C. J. Luo (Ed.), Dynamics and Vibrations of Discontinuous, Stochastic and Time Delay Systems, Springer, New York, 2010, pp. 135–157.

[110] G. P. Liu, S. Daley, Optimal-tuning nonlinear PID control of hydraulic systems, Control Engineering Practice 8 (9) (2000) 1045–1053.

[111] S. Panda, Multi-objective PID controller tuning for a FACTS-based damping stabilizer using non-dominated sorting genetic algorithm-II, International Journal of Electrical Power & Energy Systems 33 (7) (2011) 1296–1308.

[112] B. Song, J. Q. Sun, Lowpass filter-based continuous-time approximation of delayed dynamical systems, Journal of Vibration and Control 17 (8) (2011) 1173–1183.